OPEN ACCESS

Original research

Discovery and 3D imaging of a novel ΔNp63-expressing basal cell type in human pancreatic ducts with implications in disease

Sandrina Martens ,[1] Katarina Coolens ,[1] Mathias Van Bulck ,[1] Tatjana Arsenijevic ,[2,3] Joan Casamitjana,[4,5] Angel Fernandez Ruiz,[4,5] Abdessamad El Kaoutari ,[6,7] Jaime Martinez de Villareal,[8] Hediel Madhloum ,[1] Farzad Esni ,[9] Yves Heremans,[10] Gunter Leuckx ,[10] Harry Heimberg ,[10] Luc Bouwens ,[11] Patrick Jacquemin ,[12] Diedert Luc De Paep ,[13] Peter in't Veld ,[13] Nicky D'Haene ,[14] Christelle Bouchart ,[15] Nelson Dusetti ,[6] Jean-Luc Van Laethem ,[2,3] Wim Waelput ,[16,17] Pierre Lefesvre,[16,17] Francisco X Real ,[8] Meritxell Rovira ,[4,5] Ilse Rooman [1]

► Additional supplemental material is published online only. To view, please visit the journal online (http://dx.doi.org/10.1136/gutjnl-2020-322874).

For numbered affiliations see end of article.

Correspondence to
Dr Ilse Rooman, Laboratory of Medical and Molecular Oncology, Vrije Universiteit Brussel, Brussel, Belgium; irooman@vub.be

SM, KC and MVB contributed equally.
JC and AFR contributed equally.

SM, KC and MVB are joint first authors.

Received 20 August 2020
Accepted 20 July 2021

To cite: Martens S, Coolens K, Van Bulck M, *et al*. *Gut* Epub ahead of print: [*please include* Day Month Year]. doi:10.1136/gutjnl-2020-322874

ABSTRACT

Objective The aggressive basal-like molecular subtype of pancreatic ductal adenocarcinoma (PDAC) harbours a ΔNp63 (p40) gene expression signature reminiscent of a basal cell type. Distinct from other epithelia with basal tumours, ΔNp63$^+$ basal cells reportedly do not exist in the normal pancreas.

Design We evaluated ΔNp63 expression in human pancreas, chronic pancreatitis (CP) and PDAC. We further studied in depth the non-cancerous tissue and developed a three-dimensional (3D) imaging protocol (FLIP-IT, Fluorescence Light sheet microscopic Imaging of Paraffin-embedded or Intact Tissue) to study formalin-fixed paraffin-embedded samples at single cell resolution. Pertinent mouse models and HPDE cells were analysed.

Results In normal human pancreas, rare ΔNp63$^+$ cells exist in ducts while their prevalence increases in CP and in a subset of PDAC. In non-cancer tissue, ΔNp63$^+$ cells are atypical KRT19$^+$ duct cells that overall lack SOX9 expression while they do express canonical basal markers and pertain to a niche of cells expressing gastrointestinal stem cell markers. 3D views show that the basal cells anchor on the basal membrane of normal medium to large ducts while in CP they exist in multilayer dome-like structures. In mice, ΔNp63 is not found in adult pancreas nor in selected models of CP or PDAC, but it is induced in organoids from larger Sox9^{low} ducts. In HPDE, ΔNp63 supports a basal cell phenotype at the expense of a classical duct cell differentiation programme.

Conclusion In larger human pancreatic ducts, basal cells exist. ΔNp63 suppresses duct cell identity. These cells may play an important role in pancreatic disease, including PDAC ontogeny, but are not present in mouse models.

Significance of this study

What is already known on this subject?

- ΔNp63 has a central role in determining the basal-like subtype of pancreatic ductal adenocarcinoma.
- Different from other tissues with basal cancers, the normal pancreas reportedly does not contain (ΔNp63-expressing) basal cells.
- Current protocols for marker-based identification and three-dimensional (3D) imaging of individual (rare) cells in human archival pancreatic samples face severe limitations.

What are the new findings?

- We report a rare and atypical pancreatic duct cell that expresses ΔNp63, other basal cell markers and some g.i. stem cell markers.
- These ΔNp63$^+$ cells are more prevalent in chronic pancreatitis.
- Except after culturing medium to large ducts as organoids, we fail to detect ΔNp63$^+$ cells in murine experimental pancreatic models.
- ΔNp63 favours basal cell differentiation while limiting classical duct cell differentiation markers.
- We provide an easy to implement protocol for 3D clearing and high-resolution imaging of sizeable samples of (fresh or formalin-fixed and paraffin-embedded) human pancreas or of an entire mouse pancreas.

INTRODUCTION

Pancreatic ductal adenocarcinoma (PDAC) is a cancer of high unmet need. In several PDAC cohorts, a classical and a basal-like molecular subtype have been identified, the latter having the worst prognosis.[1] The basal-like subtype is characterised[2] and driven[3] by the basal cell transcription factor ΔNp63, an isoform of tumour protein P63 (*TP63*).[3 4] Notta *et al*, refined these insights by showing that not the basal-like A subtype, having the highest basal

Significance of this study

How might it impact on clinical practice in the foreseeable future?

- Extrapolating from knowledge in other organs, basal cells in the pancreas may have a stem cell/progenitor role, including in diseases such as basal-like or squamous pancreatic cancer.
- Application of the improved three-dimensional imaging protocol to archival clinical specimens will allow unprecedented insights in pancreatic histopathology.
- For above-mentioned diseases, we caution for findings in experimental mouse models that may not (fully) recapitulate the aetiopathogenesis.

cell markers including *TP63*, but a distinct basal-like B subtype showed the worst prognosis.[5] This illustrates our lack of knowledge on *TP63* and other basal cell markers in the pancreas.[1]

ΔNp63$^+$ basal cells can be the cells of origin of cancer in other tissues[6 7] but for the normal pancreas it is accepted that expression of *TP63* is absent.[3 8–10] This is in contrast to the bronchus, prostate, salivary gland, skin, breast and placenta,[9] where ΔNp63 is expressed by a specific cell population in normal ducts, located on the basement membrane and distinguished by specific markers among which cytokeratin (KRT) 5 and 14.[11] Furthermore, ΔNp63 is a well-studied key player in the development of stratified epithelium and an inhibitor of cell differentiation, crucial for stem cell renewal.[12 13] Accordingly, basal cells are progenitors in development, tissue homeostasis and regeneration.[11 14 15] Hence, we re-assessed ΔNp63 expression, and other basal cell markers, with a focus on healthy human pancreas and chronic pancreatitis (CP), a risk factor for PDAC.[16]

Studying the three-dimensional (3D) spatial organisation at single cell level in sizeable pancreatic samples requires tissue clearing together with fluorescent labelling and 3D imaging.[17 18] However, this approach faces several limitations when it comes to clinical specimens that are often formalin-fixed and paraffin-embedded (FFPE). Applying methods from brain research such as CUBIC, CLARITY and DISCO that were mainly used to study macroscopic changes,[19] provided suboptimal results for pancreas, particularly when using light sheet fluorescence microscopy. In addition to two-dimensional (2D) assessment of basal cell markers, we thus had to optimise protocols for a 3D approach.

Here, we report a novel rare cell population in the pancreas that expresses ΔNp63 and other basal cell markers. Contrary to human, we failed to detect this cell population in adult mouse pancreas. Yet, ΔNp63 could be induced in ductal organoids and ΔNp63 suppresses the classical duct cell differentiation programme. This discovery raises important conceptual questions about their developmental origin, fate and role in regeneration and disease, including the basal-type PDAC.

All relevant information is provided in a supplementary section.

RESULTS

Normal human pancreatic ducts harbour a rare ΔNp63$^+$ cell population that becomes more prevalent in CP and in a subset of PDAC

We first assessed the expression of ΔNp63 in organ donors without a history of pancreatic disease. In approximately half (53/113) of the donors, when one random section (67.2±6.8 mm^2) was assessed, we detected strong but rare ΔNp63 expression in ducts (figure 1A). This was confirmed by RNA in situ hybridisation for ΔNp63 and by immunofluorescence staining using an anti-P63 antibody that detects all isoforms (online supplemental figure 1). In the normal tissue, from head or tail region, ΔNp63$^+$ cells were detected as single cells in the basal lining of a duct, small clusters around ducts, a combination thereof or very rarely as single cells (online supplemental figure 2A–D), although these observations were limited by interpreting 2D sections.

On quantification, 0.006% of all cells were ΔNp63$^+$ (figure 1G), corresponding to 1.6% of all cells in ducts (online supplemental figure 2E). For the ΔNp63-positive samples, we found a random distribution in age, gender, the time in the intensive care, body mass index (BMI) (online supplemental figure 2F–I) and tissue fixation protocol (not shown). Donor characteristics did also not differ between ΔNp63-positive and ΔNp63-negative samples (online supplemental figure 2J–M). When analysing more than one FFPE block (n=4 donors with 2 to 10 FFPE blocks), at least one block harboured ΔNp63$^+$ cells. Together, this suggested that ΔNp63 cells could likely be found in the pancreas of any donor if sufficient material was analysed.

Next, we assessed CP, a condition with expansion of ducts and an established risk factor for PDAC.[16] When analysing one section per patient (228.3±17 mm^2), the majority of CP (9/11) were positive (figure 1B), with cells usually grouping near ducts and cysts (figure 1B). The occurrence of ΔNp63$^+$ cells in CP was significantly higher (0.17% of total cells (figure 1G) and 4% of duct cells (online supplemental figure 2E) compared with healthy controls. For the same size ducts, the number of ΔNp63$^+$ cells was also significantly increased compared with normal (figure 1H). Only 2.26%±2.11% of ΔNp63$^+$ cells labelled with Ki67 suggesting that their increase in CP is not due to proliferation.

Finally, we assessed a cohort of PDAC (online supplemental table 1) with on average 0.36% of all cells in a section (cancer and adjacent non-cancer) positive for ΔNp63 (figure 1C–G). We did not find a direct correlation between ΔNp63 expression in cancer cells and adjacent tissue (not shown). One-third of tumours, including adenosquamous tumours (online supplemental figure 3A,B), had larger positive areas and had the strongest staining intensity. H-scoring for ΔNp63 in cancer cells correlated with tumour differentiation (p=0.03). ΔNp63 was significantly associated with poorly differentiated tumours (p=0.00078, post-hoc Bonferroni).

In contrast to the prognostic value of the basal gene expression signature,[2 3 20] ΔNp63 as a stand-alone protein marker did not correlate with overall survival (online supplemental figure 3C), confirming a previous report on n=422 PDAC.[10] Also, the The Cancer Genome Atlas (TCGA) data set (n=150) showed no survival association with *TP63* messenger RNA (mRNA) (log rank=0.15) while it did for the other basal cell markers *KRT14* and *S100A2* (log rank=0.004 and log rank=0.008, respectively) (https://app.gebican.fr/pdac-survival/).

To further assess the correlation of ΔNp63 expression with the basal-like signature, we took advantage of n=44 PDAC cell lines,[21] allowing to directly assess the epithelial component of the tumour. All other transcriptomic studies referred to *TP63* (ENSG00000073282), whereas here we specifically distinguished the ΔN-isoform (ENST00000354600). When using the pancreatic adenocarcinoma molecular gradient (PAMG), which reflects gradually the molecular subtypes from the most basal-like to the most classical,[22] we confirmed a negative correlation (Pearson's coefficient R=−0.34, p=0.023) with ΔNp63 (online supplemental figure 3D). Also, in a PurIST binary classification, levels of ΔNp63 expression are significantly higher in basal

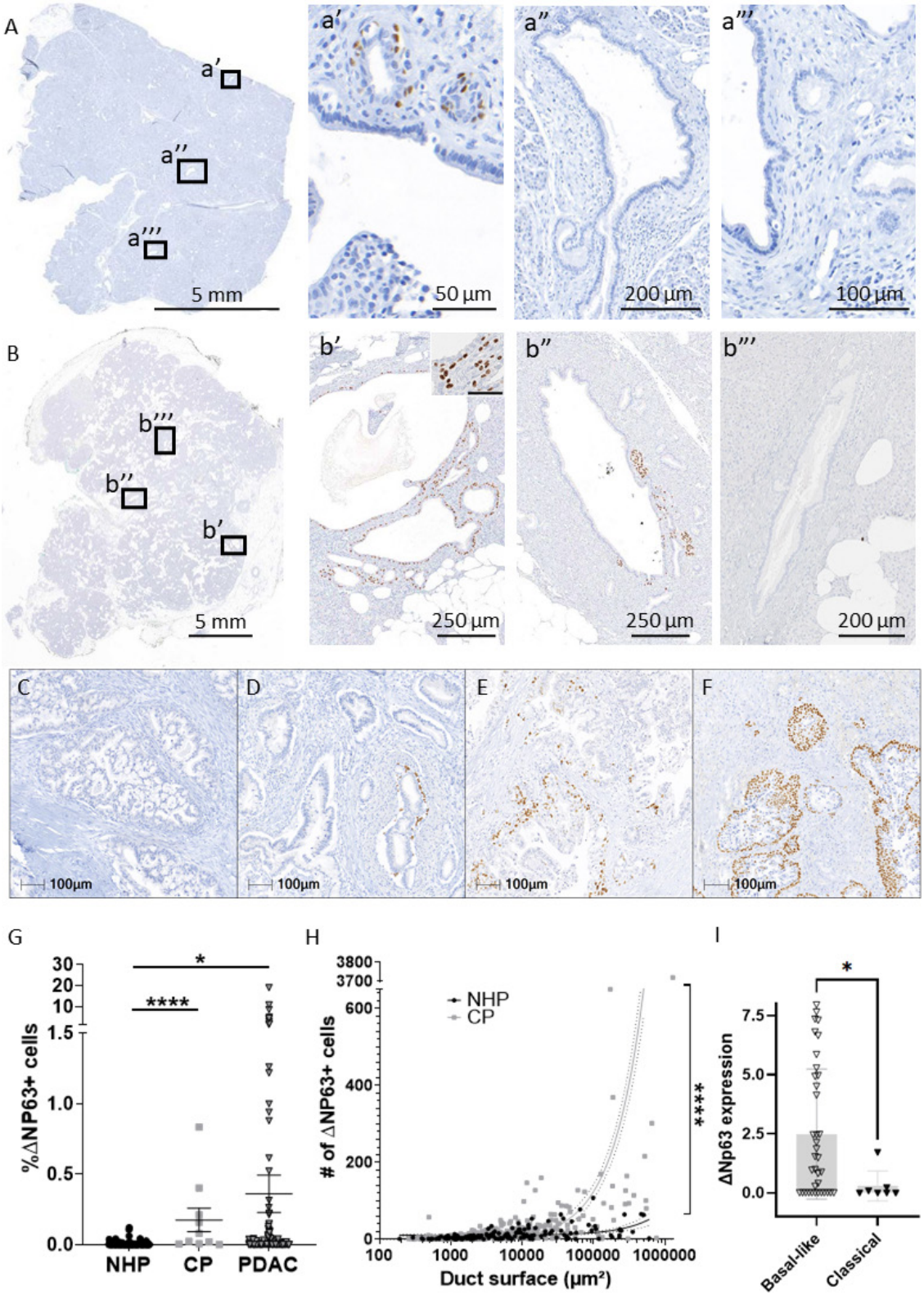

Figure 1 Normal human pancreatic ducts harbour a rare ΔNp63$^+$ cell population that becomes more prevalent in CP and in a subset of PDAC. (A) ΔNp63 staining in one representative section of NHP (n=114): Three ductal areas are shown, of which one (a′) contains a limited number of positive cells, and two other areas (a″ and a‴) are negative. (B) ΔNp63 staining in one representative section of human CP (n=11). Three ductal areas are shown, of which two (b′ and b″) contain a high number of positive cells, and one area (b‴) is negative. An inset is shown in (b′). (C–F) Representative images of the stainings in a PDAC cohort (n=141), displaying four different tumour groups: (C) negative tumour, (D) partially positive tumour, showing basal cells in one duct, (E) positive tumour and (F) adenosquamous tumour. (G) Quantification of the percentage of ΔNp63$^+$ cells in whole tissue sections from NHP, CP and PDAC. *p<0.05, ****p<0.0001. (H) Quantification of the number of ΔNp63$^+$ cells in ΔNp63$^+$ ducts from NHP and CP. ***p<0.0001. (I) ΔNp63 expression in basal-like (n=37) versus classical subtype (n=7) PDAC cell lines (Error bars indicate SD). *p<0.05. CP, chronic pancreatitis; NHP, normal human pancreas; PDAC, pancreatic ductal adenocarcinoma.

versus classical PDAC (p=0.036) but, interestingly, a proportion of basal-like PDAC do not express any ΔNp63 (figure 1I and online supplemental figure 3D).

We thus report for the first time the occurrence of rare ΔNp63-expressing cells in normal human pancreatic ducts. Their presence is significantly higher in CP and in a subset of PDAC. The ΔNp63 isoform correlates with the basal-like gene expression signature in PDAC but cannot be used as a reductionist (prognostic) marker.

ΔNp63$^+$ cells are distinct from normal pancreatic duct cells and display typical basal cell markers

To determine the identity of ΔNp63-expressing cells, we analysed the expression of an epithelial marker (E-cadherin), canonical pancreatic duct cell markers (KRT19, CA19.9, SOX9, HNF1β, KRT7) and a marker of pancreatic duct glands (MUC6), a suggested stem cell niche.[23] In addition, we analysed basal cell markers (KRT5, KRT14 and S100A2)[11 24 25] as well as basal positioning, pale cytoplasm and nuclei.[26] In breast, myoepithelial cells express ΔNp63 as well as myogenic markers.[27] So, we also analysed calponin and alpha smooth muscle actin (aSMA). All results shown below were made on CP because of the convenience of having more ΔNp63$^+$ cells but the described staining patterns overall did not differ in the rare ΔNp63$^+$ cells in normal pancreas (online supplemental table 2).

P63$^+$ cells were positive for E-cadherin (online supplemental figure 4) and KRT19 (figure 2A) but not for CA19.9 (figure 2B). Nuclear expression of SOX9 and HNF1B was rare, while all the neighbouring P63$^-$ duct cells stained positive (figure 2C,D). P63$^+$ cells also lacked ductal KRT7 (figure 2E).

On a haematoxylin-eosin saffron (HES) staining (online supplemental figure 5A–D), P63$^+$ cells often presented with a basal location, a paler cytoplasm and paler nuclei, compared with P63$^-$ cells. All P63$^+$ cells strongly expressed KRT5 (figure 2F), while a subset expressed KRT14 (figure 2G). A large subset was S100A2$^+$, a direct transcriptional target of ΔNp63[28] (figure 2H), similar to prostate and airway basal cells.[24 25] The pancreatic P63$^+$ cells did not express MUC6 (online supplemental figure 5E,F) and MUC6 did not overlap with the other basal marker KRT5 (online supplemental figure 5G). Additionally, the cells were negative for aSMA and calponin (online supplemental figure 5H–K).

In conclusion, pancreatic ΔNp63$^+$ cells display a phenotype reminiscent of canonical basal cells from other tissues and represent a population of atypical ductal cells.

Ducts containing ΔNp63$^+$ cells express gastrointestinal stem cell markers

In other epithelia, basal cells are thought to be progenitors. Therefore, we investigated gastrointestinal (GI) stem cell markers including DCLK1, CD142 and OLFM4[29–31] in addition to more general, pluripotent stem cell markers (NANOG, OCT4).

Most basal P63$^+$ cells were DCLK1$^+$ (figure 3A). Singular DCLK1$^+$ P63$^-$ cells were also observed, confirming previous reports in pancreas[32 33] (figure 3B). Basal cells and some neighbouring luminal cells, specifically of ducts containing P63$^+$ cells, expressed CD142 while CD142 was not found in ducts lacking P63$^+$ cells (figure 3C,D). OLFM4 was absent in P63$^+$ cells and rarely expressed in neighbouring cells (figure 3E). However, we found it exclusively in the lumen of ducts containing P63$^+$ cells (figure 3E,F) and could discard this as being bile (not shown). The cells did not express NANOG or OCT4, in contrast to positive control samples (online supplemental figure 6).

In summary, ducts containing pancreatic basal cells show expression of some GI stem cell markers, either in the basal cells, in the juxtaposed cells or both, suggesting the basal cells pertaining to a stem cell niche.

FLIP-IT allows 3D visualisation of pancreatic basal cells in archival FFPE tissue

Another distinct feature and function of basal cells is the anchoring to the basal membrane.[34] To visualise this, 3D imaging with high magnification and high numerical aperture objectives in conjunction with highly cleared samples and preservation of fluorescence intensity is required. Thus far, imaging at a high magnification (≥20×) could only be achieved with lengthy confocal or two-photon microscopy thus limiting the scanning capabilities, increasing the scanning time and inducing extensive photobleaching.[35 36]

Hence, we developed a protocol for Fluorescence Light sheet microscopic Imaging of Paraffin-embedded or Intact Tissue (FLIP-IT) with optimised permeabilisation and delipidation based on sodium dodecyl sulfate delipidation buffers. For the Refractive Index matching, we used the complementary effect of CUBIC-R (CUBIC) and ethyl cinnamate (ECi). FLIP-IT enabled us to assess FFPE and intact (fresh) tissues from patients and mice (figure 4A, online supplemental figures 7 and 11) at unmet speed, that is, the process from clearing to imaging was completed in less than 2 weeks, much faster than published methods[19] (see also online supplemental methods). ECi also preserved the fluorescent signal for months.

Rare P63$^+$ cells could be found as solitary cells in or as clusters attached to ducts with a minimal diameter of 20 micron (figure 4B). Solitary P63$^+$ cells lie between the basal lamina and the luminal cells of large ducts and P63$^+$ clusters also associated to the basal lamina (figure 4C). In contrast, in CP, KRT19$^+$ domes of multiple cell layers formed around a lumen, where only the basally located P63$^+$ cells touched the basal membrane (figure 4D,D').

Because of the overlap between P63 and KRT5 (figure 2F) and the mutual exclusive expression of KRT5 and KRT7, both cytoskeletal markers that allow a good appreciation of cell morphology, 3D image rendering was used for straightforward identification of KRT5$^+$ KRT7$^-$ basal cells (online supplemental video 1 and figure 5A). Small clusters of round basal cells in normal pancreas (n=4, one punch each) were grouped around a small lumen (figure 5C,C'). In CP (n=2, two punches each) (online supplemental video 1 and figure 5B), large dome-like clusters associated to cystic ducts and were already apparent from the overview 3D rendering, with KRT5$^+$ cells located at the outside of the domes and KRT7$^+$ cells lining the lumen (figure 5D,D'). 3D measurements of sphericity and volume at single cell level demonstrated that the domes consisted of flatter cells and that the cell volume of the KRT5$^+$ cells had increased in CP (online supplemental figure 8).

Thus, leveraging on a novel imaging protocol, FLIP-IT, that is widely applicable, we established the spatial distribution and morphometric features of individual pancreatic basal cells within the ductal tree, in normal pancreas and CP.

ΔNp63 expression is undetectable in commonly used mouse models of pancreatic disease but is acquired by a subset of SOX9^{low} duct cells

We re-assessed ΔNp63 expression in adult mouse pancreas since single-cell RNA sequencing studies did not provide evidence for its expression (online supplemental table 3). In contrast to mouse

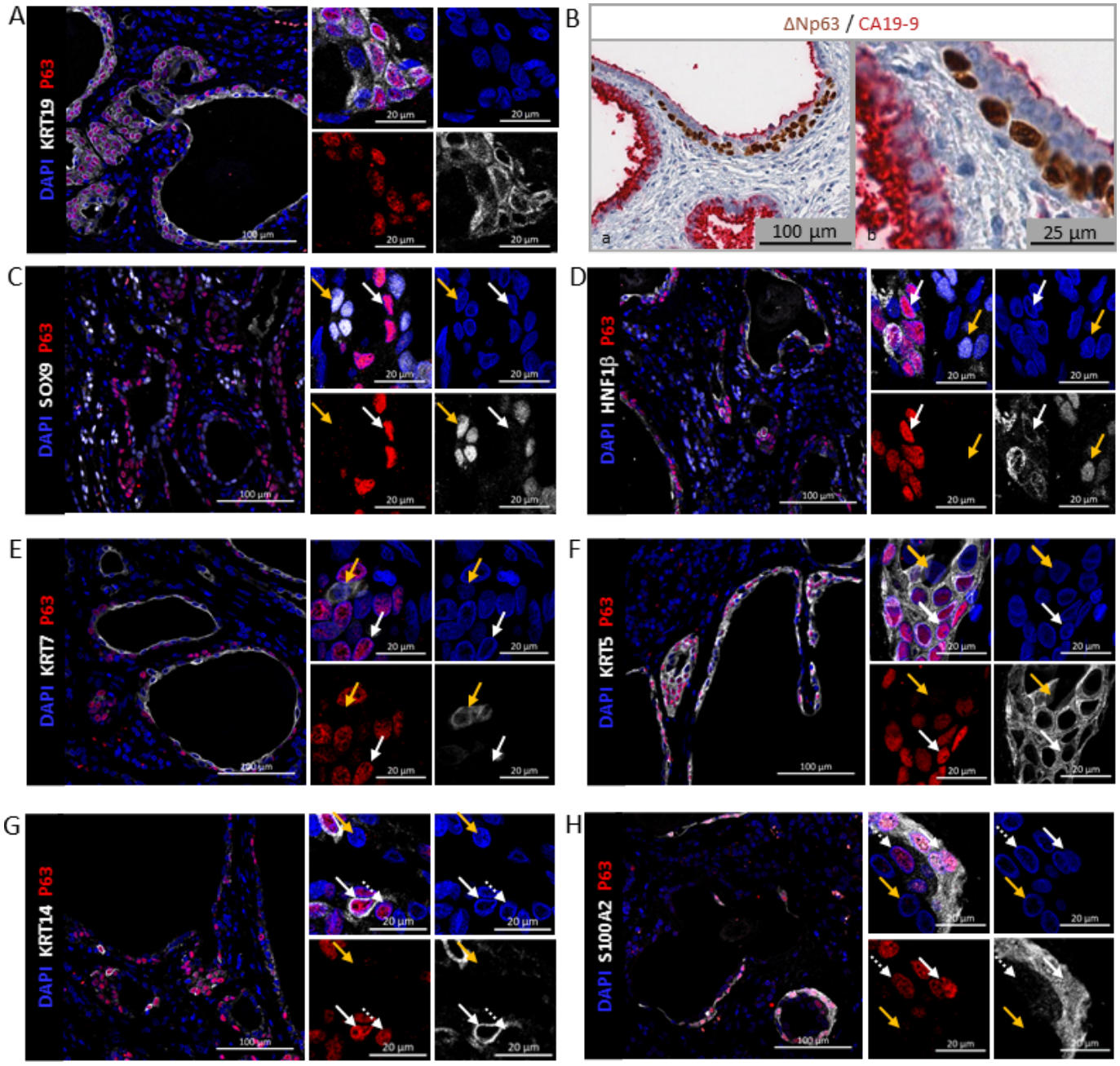

Figure 2 ΔNp63$^+$ cells are distinct from normal pancreatic duct cells and display typical basal cell markers. (A) IF for KRT19 (white) and P63 (red), showing co-expression; (B) IHC for ΔNp63 (brown) and CA19.9 (red). CA19.9 expression is absent in ΔNp63$^+$ cells and weaker in the duct lumen (see inset); (C) IF for SOX9 (white) and P63 (red). SOX9$^+$ cells are indicated with an orange arrow, while P63$^+$ cells are indicated with a white arrow; (D) IF for HNF1B (white) and P63 (red). HNF1B$^+$ cells are indicated with an orange arrow, while P63$^+$ cells are indicated with a white arrow; (E) IF for KRT7 (white) and P63 (red). White arrow indicates a P63$^+$ cell, while the orange arrow indicates a KRT7$^+$ cell; (F) IF for P63 (red) and KRT5 (white). White arrow indicates a P63$^+$ cell, orange arrow indicates a P63$^-$ cell; (G) IF for P63 (red) and KRT14 (white). Solid white arrow indicates a P63$^+$KRT14$^+$ cell, dotted white arrow indicates a P63$^+$KRT14$^-$ cell. Orange arrow indicates a P63$^-$ cell; (H) IF for S100A2 (white) and P63 (red). Solid white arrow indicates a P63$^+$S100A2$^+$ cell, dotted white arrow indicates a P63$^+$S100A2$^-$ cell. Orange arrow indicates a P63$^-$ cell. IF, immunofluorescence; IHC, immunohistochemistry.

mammary gland and skin (online supplemental figure 9), ΔNp63 was undetectable in pancreas, even when assessing over 4×10^6 duct cells with artificial intelligence (AI)-assisted identification of duct cells, including larger ducts such as the main pancreatic duct and the common bile duct (online supplemental figure 10). The 95% CI for the number of ΔNp63$^+$ cells per sample ranges from 0 to maximum $3.633031e^{-06}$ (meta-analysis) or $1.215163e^{-07}$ (Clopper-Pearson). Hence, we have no reason to assume that ΔNp63$^+$ cells exist in the adult mouse pancreas. If they do, their occurrence is too limited to deduce meaningful information unless after analysing very large sample sizes. Similarly, we did not find ΔNp63$^+$ cells in pancreas from pregnant, postpartum, neonatal and aged mice (figure 6A). We also analysed experimental models of CP, that were, caerulein-treated (treatment up to 8 weeks, analysis up to 14 weeks after treatment) or duct-ligated *Kras*^{WT} mice and caerulein-treated *Kras*^{G12D} (KC) mice.[37] ΔNp63 was undetectable here as well

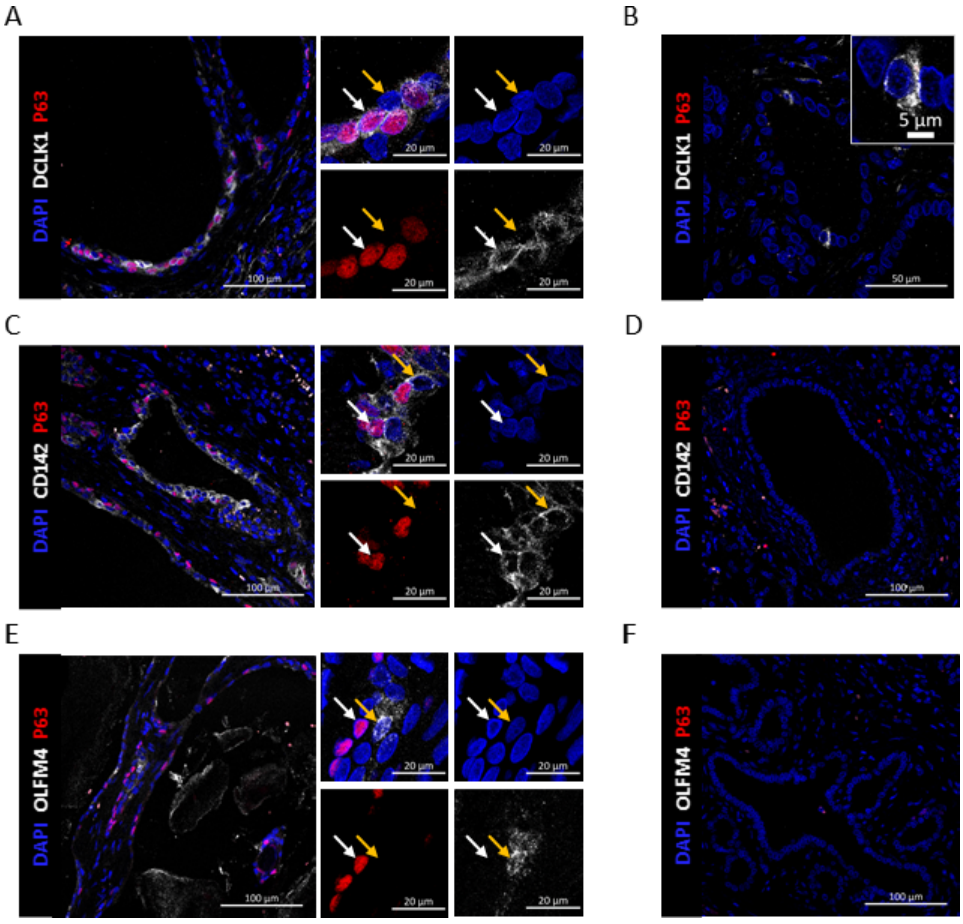

Figure 3 Ducts containing ΔNp63$^+$ cells express gastrointestinal stem cell markers. (A) IF for DCLK1 (white) and P63 (red). P63$^+$ cells express DCLK1 but are not like tuft cells (B) that are solitary cells with apical microvilli and devoid of P63; (C) IF for P63 (red) and CD142 (white). P63$^+$ cells and the cells located at the apical side of P63$^+$ cells express CD142, unlike ducts without P63$^+$ cells (D); (E) IF for P63 (red) and OLFM4 (white). Ducts that contain P63$^+$ cells secrete OLFM4 into their lumen (indicated with asterisk) and rarely contain OLFM4$^+$ cells, unlike ducts that do not contain P63$^+$ cells (F). IF, immunofluorescence.

as in tumours from *Kras* and *Trp53* mutant KPC mice.[37] All these samples were also negative for KRT5 and KRT14 (not shown). 3D imaging of a whole mouse pancreas, including the main duct (online supplemental figure 11) confirmed the absence of KRT5$^+$ cells. In addition, *Krt14*-eGFP mice showed no KRT14 by GFP or KRT14 staining (skin was positive, not shown). Also, adult rat (n=7) and pig pancreas (n=3) were negative.

We next investigated organoid cultures that favour a progenitor cell-like phenotype. We used ductal cell digests from *Sox9*-eGFP reporter mice.[38] These preparations showed intrinsic heterogeneous SOX9 expression with larger ducts having lower expression (figure 6B). Cell fractions were produced according to eGFP expression level, corresponding to the size of the ducts. None of the freshly isolated cell fractions showed Δ*Np63* expression by real-time quantitative PCR (figure 6C), confirming our histological analyses (figure 6A). On organoid culture, cells from SOX9^{low} medium to large size ducts showed an upregulation of Δ*Np63* (figure 6C), as well as of *Krt5* and *Krt14* mRNA (not shown) gene expression. Whole mount staining of organoids confirmed a heterogeneous pattern of p63 protein expression that correlated with the lowest levels or with near absence of SOX9 (figure 6D and online supplemental video 2), reminiscent of the findings in human pancreas. P63$^+$ cells showed little proliferation, as observed by 5-ethynyl-2′-deoxyuridine (EdU) labelling (online supplemental figure 12). Different from p63, Krt5 and 14 were not detected. Thus, organoids from larger ducts activate basal markers but do not fully acquire a basal phenotype.

In conclusion, while normal adult mouse pancreas and commonly used models of CP and PDAC do not show basal cells. Organoid cultures established from larger pancreatic ducts can acquire ΔNp63 expression, pointing at plasticity in duct cell differentiation.

ΔNp63 supports a basal differentiation state while repressing classical duct cell identity

HPDE cells, obtained after immortalisation of cells from larger human pancreatic ducts,[39] express ΔNp63 (online supplemental figure 13A,C), hitherto unreported. TAp63 is also expressed, however at lower levels (not shown). Hence, HPDE cells provided a useful proxy to decipher the role of ΔNp63 in the pancreatic duct cell. Four different small interfering RNAs (siRNAs) gave efficient knockdown (KD) of ΔNp63 (online supplemental figure 13B), with the one against the ΔN isoform validated at protein level (online supplemental figure 13C). RNAseq analysis of the KD experiment highlighted 1593 differentially expressed genes (online supplemental table 4). Of these, *TP63* and another 748 genes were downregulated and 844 genes were upregulated (figure 7A). The top upregulated genes feature

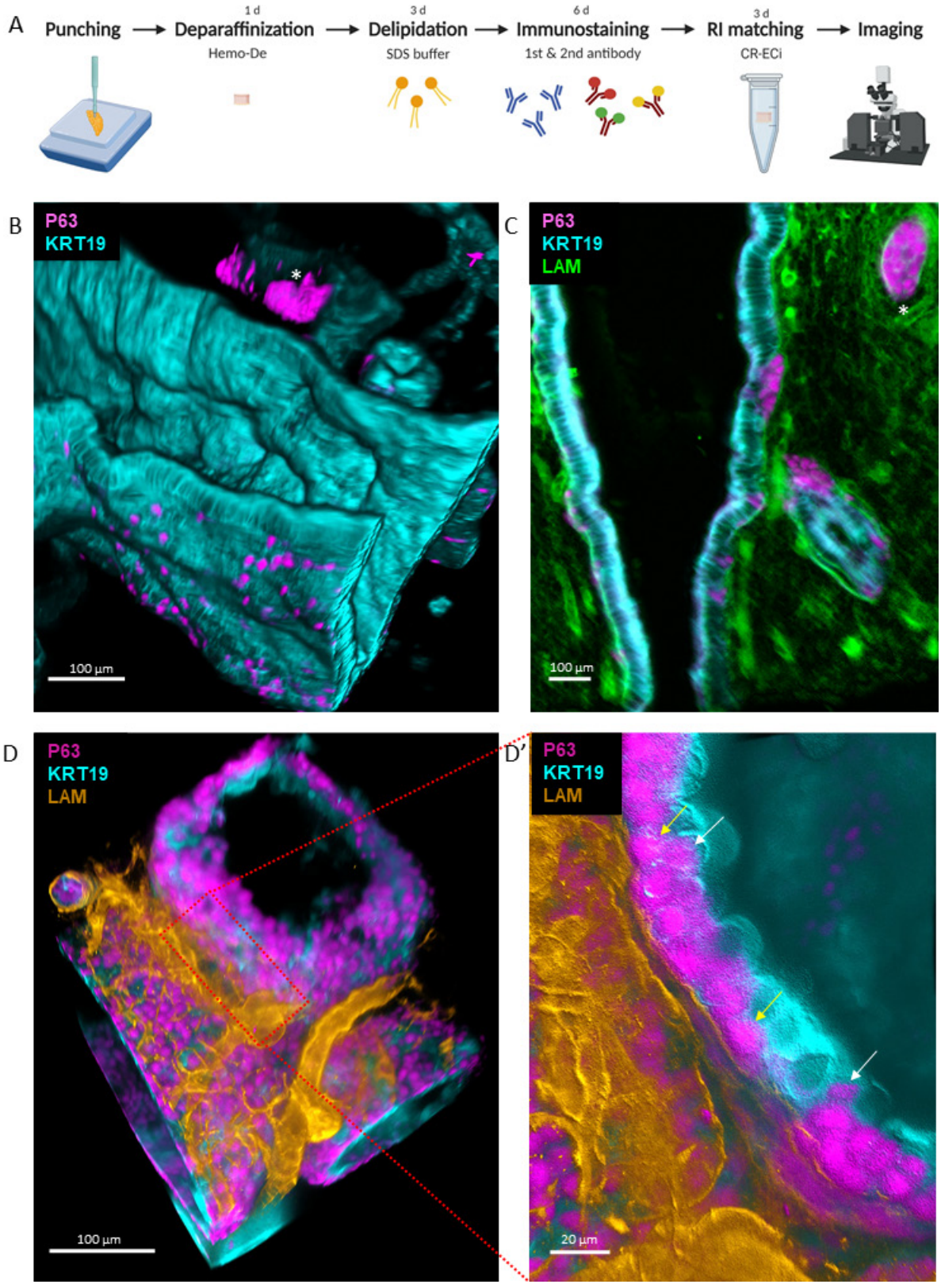

Figure 4 FLIP-IT allows 3D visualisation of pancreatic basal cells in archival FFPE tissue. (A) Overview of the FLIP-IT protocol for processing of human archival FFPE samples; (B) Overview 3D volume rendering of a large duct system (cyan) with P63^{+} cells (pink) in normal human pancreas. Objective 20×, zoom 0.36. Scale bar corresponds to 100 µm; (C) Z-plane clipping of B with KRT19 (cyan), P63 (pink) and laminin (green). Asterisk indicates reference structure in B. Objective 20×, zoom 0.36. Scale bar corresponds to 100 µm; (D) Overview 3D volume rendering of a dome positive for P63 (pink) in CP. Objective 20×, zoom 1. Scale bar corresponds to 100 µm. (D') Inset from D. Yellow arrows indicate P63^{+} (pink) cells in contact with the basal membrane (orange). White arrows indicate P63^{+} cells not in contact with the basal membrane. Objective 20×, zoom 1. Scale bar corresponds to 20 µm. n≥2. CR-ECi, CUBIC-R-ethyl cinnamate; FFPE, formalin-fixed and paraffin-embedded; FLIP-IT, Fluorescence Light sheet microscopic Imaging of Paraffin-embedded or Intact Tissue; RI, Refractive Index; 3D, three-dimensional.

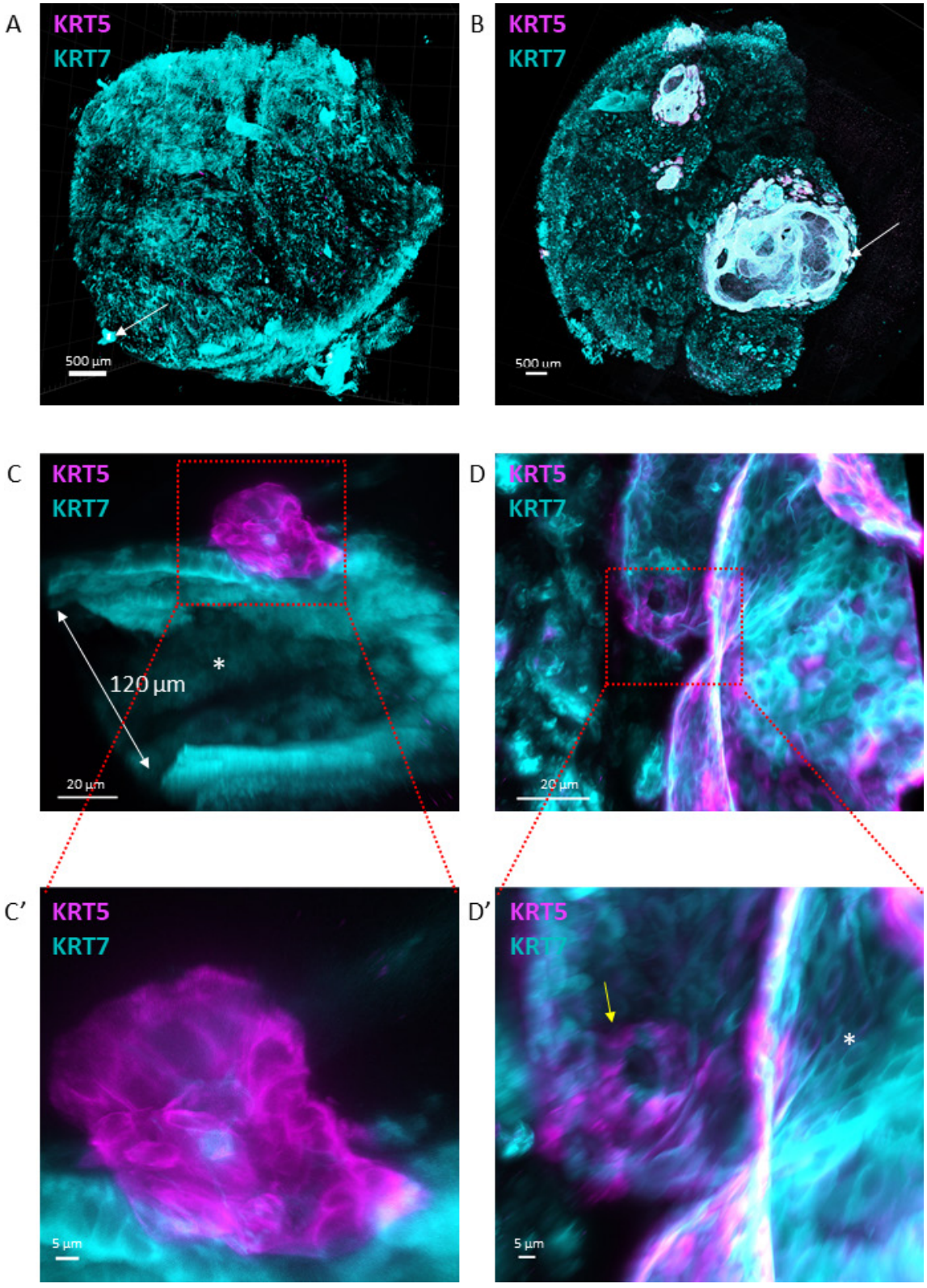

Figure 5 3D imaging of KRT5-positive basal cells in NHP and expansion as dome-like structures in CP. (A) Overview 3D rendering of NHP and (B) CP from FFPE blocks stained for KRT5 (pink) and KRT7 (cyan). Arrows indicate magnified regions in (C) and (D). Objective 20×, zoom 0.36. Scale bar corresponds to 500 µm; (C) HR-LSFM of a KRT5$^+$ (pink) dome on a large KRT7$^+$ (cyan) duct with lumen diameter 120 µm at its widest point in normal pancreas. Asterisk indicates lumen. Objective 20×, zoom 2.5. Scale bar corresponds to 20 µm; (D) HR-LSFM of dome wall showing its constitution in CP. Objective 20×, zoom 2.5. Scale bar corresponds to 20 µm; (C') inset from C showing in detail the cellular structure of KRT5$^+$ (pink) cells in NHP. Objective 20×, zoom 2.5. Scale bar corresponds to 5 µm; (D') HR-LSFM of dome wall showing flat KRT5$^+$ (pink) and KRT7$^+$ (cyan) cells intercalated (yellow arrow) and KRT5$^+$ (pink) cells lining the exterior of the dome wall. Asterisk indicates lumen. Objective 20×, zoom 2.5. Scale bar corresponds to 5 µm. n≥2. 3D, three-dimensionalCP, chronic pancreatitis; FFPE, formalin-fixed and paraffin-embedded; HR-LSFM, high-resolution light sheet fluorescence microscopy; NHP, normal human pancreas.

A

Mouse model	Background strain	mice N=	sections/sample N=
Healthy WT mouse	C57BL/6J	8	2
Healthy WT mouse	CD-1	6	2
Dissected area of fusion of common bile duct and main pancreatic duct	CD-1	3	1
Aged mouse (76 - 114 weeks)	C57BL/6	6	1
KRT14 transgenic mouse	C57BL/6	4	1
Pregnant mouse	CD-1	2	3
Postpartum mouse	CD-1	2	3
Neonatal mouse	C57BL/6	4	1
Pancreatic Duct Ligated (PDL) mouse	BALB/c	8	2
Caerulein treated WT mouse	129 Sv/C57BL/6	14	2
Caerulein treated KC mouse	Cross C57BL/6 and BALB/c	8	1
KPC mouse	129 Sv/C57BL/6	5	1

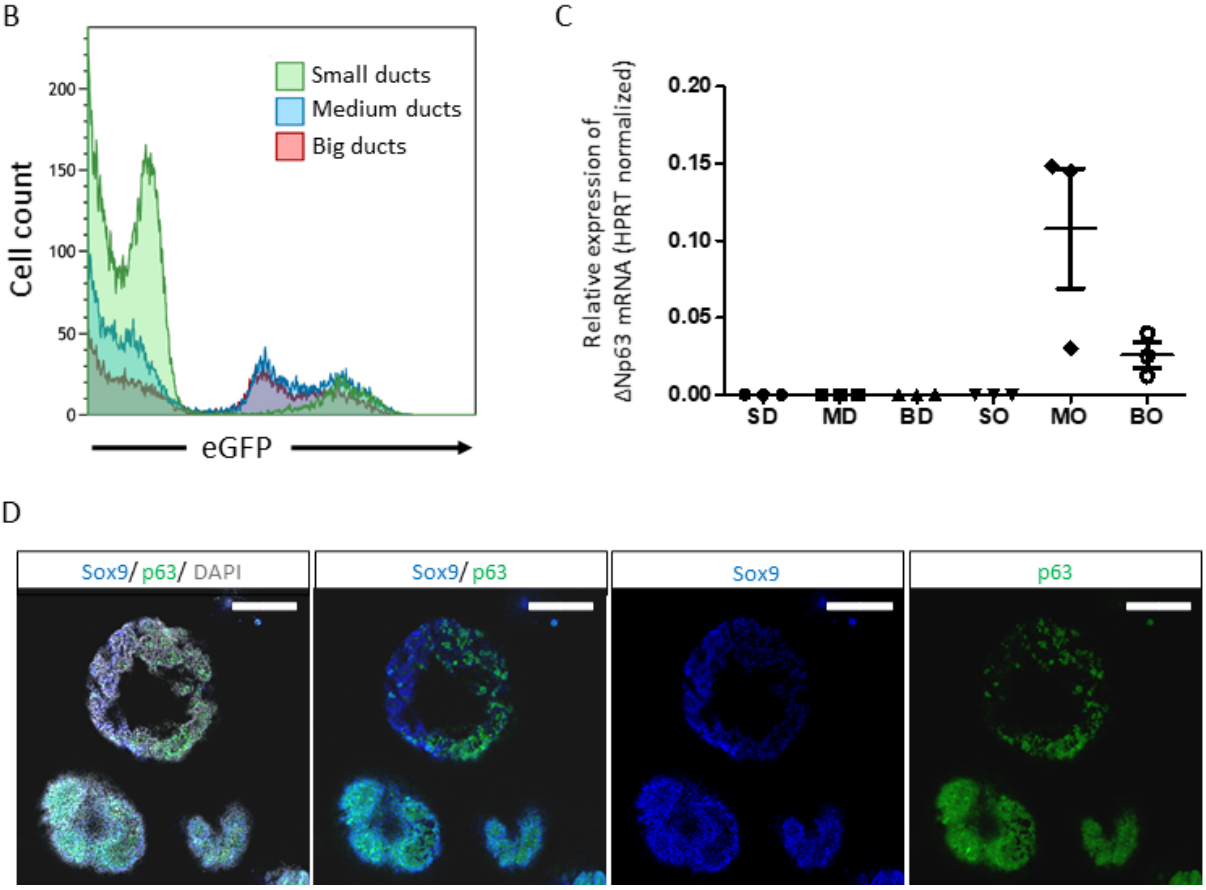

Figure 6 ΔNp63 is induced in mouse pancreatic organoids but is undetectable in normal mouse pancreas and in mouse pancreatic disease models. (A) Table summarising mouse models used to investigate ΔNp63 expression using immunohistochemistry staining for ΔNp63, Krt14 and Krt5. Background strain is indicated for each separate mouse model. Number of mice analysed, and sections analysed per sample are indicated. (B) Representative flow cytometry plot of ductal cells isolated from *Sox9*:eGFP reporter mice, showing different levels of *Sox9*:eGFP expression that inversely correlate with the size of the ducts. (C) Bar plot indicates *ΔNp63* mRNA levels normalised to *Hprt* of mouse ducts of different sizes (BD, big duct; MD, medium duct; SM, small duct) and organoids derived of the aforementioned ducts (organoids derived from BO, big ducts; MO, medium ducts; SO, small ducts). Error bars indicate SD of three independent experiments. (D) Representative immunofluorescence staining of p63 (green) and Sox9 (blue) of organoids derived from big to medium sized ducts. Nuclei are stained grey (DAPI). Scale bar=200 µm. mRNA, messenger RNA; WT, wild type.

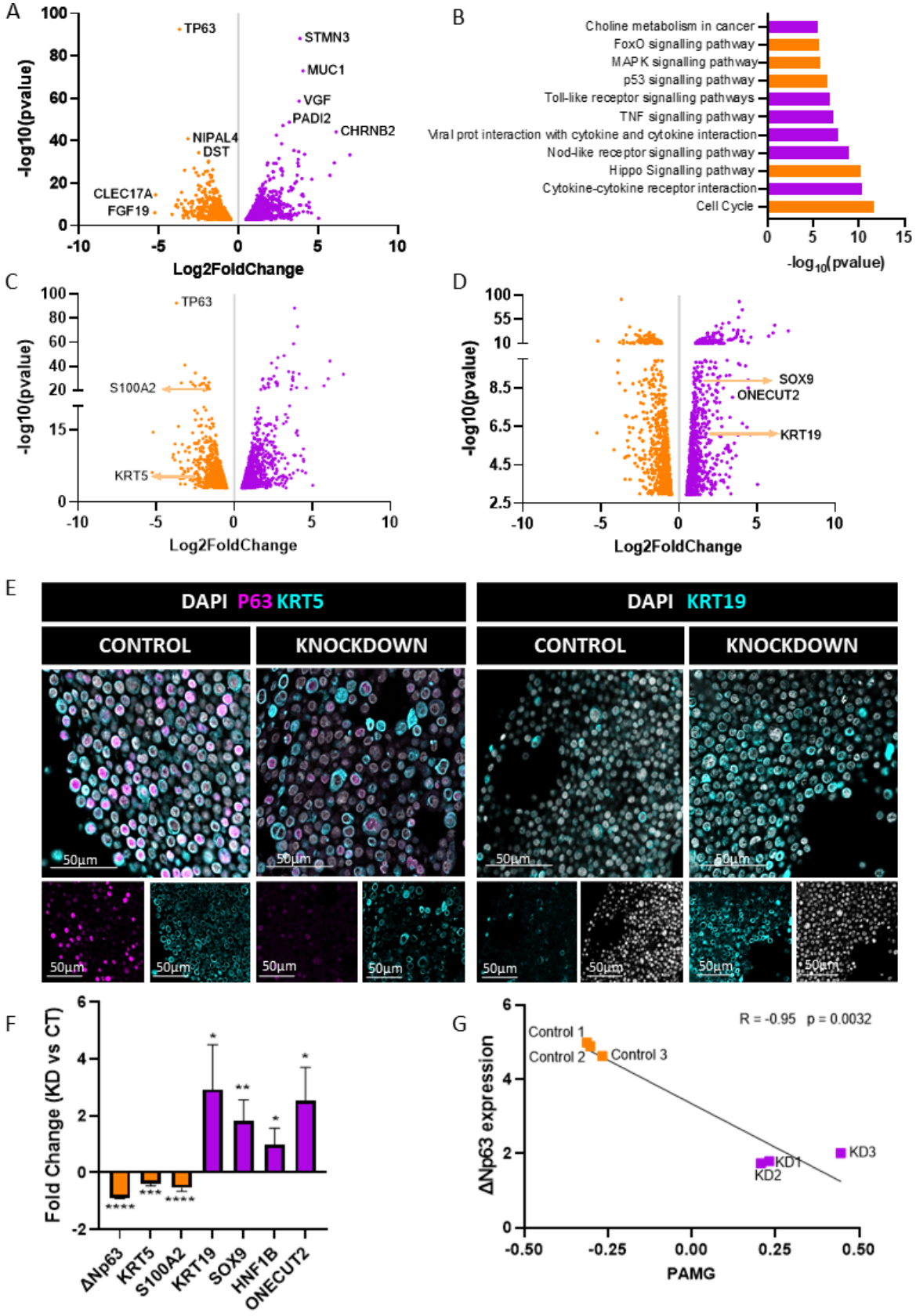

Figure 7 ΔNp63 maintains a basal cell differentiation state while repressing duct cell identity. (A) Volcano plot and (B) KEGG pathway analysis of differentially expressed genes after KD of ΔNp63^{+} in HPDE cells (n=3, p<0.01 and FDR<0.01). In orange, the pathways represented by downregulated genes, in purple those from the upregulated genes. (C) Volcano plot of basal and (D) of ductal markers in the same RNAseq data. (E) Confirmation of basal (P63 and KRT5) and classical ductal marker KRT19 by immunofluorescence staining and (F) quantitative RT-PCR (*p<0.05; **p<0.01; ***p<0.001; ****p<0.0001). (G) Correlation of PAMG scores in ΔNp63 KD (purple) and control (orange) HPDE samples (R =–0,95, p=0.0032). FDR, false discovery rate; KD, knockdown; PAMG, Pancreatic Adenocarcinoma Molecular Gradient.

MUC1 and *PADI2*, known pancreatic duct cell genes,[40] as well as several endocrine genes. Downregulated genes were enriched for the KEGG pathways 'Cell cycle' and 'Hippo Signalling Pathway', consistent with the reported roles of ΔNp63 and basal cells,[4 41 42] whereas upregulated genes featured in 'Cytokine-cytokine receptor interaction' and 'metabolic pathways'. Next to *MUC1*, other duct cell genes such as *SOX9* appeared upregulated while basal cell genes were downregulated (figure 7C,D), as confirmed by immunofluorescence staining and qRT-PCR, and validated for other siRNAs (figure 7E,F and online supplemental figure 13D). KD of ΔNp63 in the mouse duct-derived organoids confirmed upregulation of SOX9, HNF1B and, to some extent, KRT19, especially in medium-sized duct organoids (online supplemental figure 13E). Finally, to confirm the association of ΔNp63 with basal gene expression and repression of 'classical' duct cell genes, we assessed the PAMG scores. The results showed that after ΔNp63 KD, the cells shifted from a basal-like to a classical phenotype (figure 7G). These findings highlight that ΔNp63's described role in PDAC[3] also applies to normal duct cells.

We conclude that concurrent with its known master regulatory function in suppressing epithelial cell differentiation, ΔNp63 also suppresses pancreatic duct cell differentiation in favour of a basal differentiation programme.

DISCUSSION

Despite a consensus on the existence of a basal-like molecular subtype of PDAC driven by ΔNp63,[3] it is widely accepted that ΔNp63-expressing cells do not exist in healthy human and mouse pancreas.[3 8–11] Here, we provide compelling evidence of a ΔNp63$^+$ cell population in the pancreas of individuals without a history of pancreatic disease. The lack of association with socio-demographic and clinical parameters suggests that this cell fate is a constitutive feature of normal pancreatic differentiation.

The location of ΔNp63$^+$ cells between the basal membrane and the luminal duct cells and their expression of KRT5, KRT14 and S100A2 shows that they are the counterpart of basal cells from other epithelial tissues. Like airway basal cells, they are either KRT14$^+$ or KRT14$^-$, while they are all KRT5$^+$.[43] KRT5 and KRT14 were reported in the human pancreas[44] in less than 5% of ductal cells, corresponding with our findings. Studies using transmission electron microscopy reported a basally located cell type in human and rat pancreas, which were suggested to be a source of new ductal cells.[45 46] Previous studies were likely limited by the lack of large collections of normal pancreata. Altogether, our findings call for a re-evaluation of the concept that the pancreatic duct is a homogeneous 'simple epithelium', as established in classical histology textbooks.

The ΔNp63$^+$ basal cells of the pancreas are situated in the ductal tree and express KRT19[44–47] but the overall absence of CA19.9, SOX9 and HNF1B indicate that these cells represent a novel pancreatic duct cell type. Single-cell RNA sequencing (scRNAseq) has failed to provide evidence thereof. A recent paper on human duct cell heterogeneity[48] did not report cells with basal cell characteristics, possibly because only ALK3$^+$ cells were analysed and ALK3 itself has not been reported in basal cells.[24] Other scRNAseq of human pancreas[49 50] did not pick up (ΔN)p63 either. The rarity of ΔNp63$^+$ cells, their restricted distribution along the ductal tree and the shallowness of current scRNAseq likely account for this. In one data set, we detected rare ΔNp63$^+$ cells in patients with type 2 diabetes,[51] reaffirming their increased presence in disease.

We established a 3D imaging pipeline that allowed for the first time assessing cubic millimetres of a clinical sample or a whole mouse pancreas. Using FLIP-IT with punches of archival samples, we visualised the ductal tree and confirmed the existence of rare basal cells in ducts with a minimal diameter of 20 µm. In CP, these cells were differently organised as larger multilayer dome structures that could reach sizes of cubic millimetre order. Thus FLIP-IT allows for unprecedented 3D views of cells stained for markers of choice, endowing researchers with a wealth of information on (pancreatic) histopathology. We envision that this new approach can also inform about the exact positioning of, for example, stromal cell types versus tumour epithelium.

In contrast to human tissue, we failed to detect any basal cell in the adult mouse pancreas, including several disease models in which other organs activate such population.[52 53] Bearing in mind that Sox9 in human pancreatic basal cells was rare, we assessed mouse pancreatic duct cells according to their variable Sox9 expression. Indeed, only when culturing the Sox9^{low} duct cells under stem cell-favouring organoid conditions, ΔNp63 expression was induced. This illustrated an inherent potential of duct cells to turn on a basal cell phenotype. However, our data suggest that published work might have missed this important cell type when using murine tissue. If basal cells were to exist in mice, using *Sox9* and *Hnf1b* as Cre-drivers may not be adequate models. *Krt19*-Cre might be more suitable since all pancreatic basal cells, at least in human, express KRT19.

Our findings warrant studies on pancreatic basal cells in homeostasis and disease. Pancreatic stem cells have been disputed and have been mostly studied in the context of β-cell regeneration. Only after substantial tissue injury, (facultative) stem cells appear to become activated.[54] It is conceivable that basal cells would be a different and 'last resort' stem cell, similar to skin and intestine, where different types of stem cells reside in restricted niches. In pancreas this niche appears to express markers of GI stem cells. Commonly for such cells, their full potential is not called upon under normal physiological conditions, only specific conditions may recruit these cells.[55] The organoid culture conditions could have provoked such response. Interestingly, SOX9$^-$ cells in the ductal tree seem to contribute to new β-cells[56] and a SOX9-dosage effect mediates adult duct cell identity.[57] We find a broader duct cell plasticity regulated by ΔNp63 in HPDE where ΔNp63 favours the basal cell fate at the expense of differentiated duct cell markers, including but not restricted to suppression of SOX9. It remains speculative whether ΔNp63 expression in HPDE is due to the cell of origin being a basal cell or being acquired on immortalisation and inactivation of *TP53*.

We demonstrate that pancreatic basal cells are more abundant in CP suggesting an active contribution to its pathogenesis. With the very low rate of proliferation and conscious of the duct cell plasticity discussed above, our data suggest that this increase is due to altered cell differentiation rather than proliferation of pre-existing basal cells. Early-stage samples of disease would facilitate such study but are scarce. In absence of mouse models, development of human modelling systems, for example, using purified basal cells from adult human pancreas, would be very valuable.

One clear gap of knowledge is the development of subtypes of PDAC. Their ontogeny and plasticity could be driven by oncogenic mutations and by environmental stress but could also be the cell of origin. Murine pancreatic acinar and duct cells can generate tumours[1 58] and different PDAC phenotypes share traits with the cells of origin where (epi)genetic features of duct cells are retained in the more aggressive basal subtype.[59 60] Our findings call for considering the role of basal cells. The inverse

correlation of ΔNp63 and SOX9 expression is also reminiscent of our previous work where the basal subtype showed the lowest SOX9 expression.[61] We now added that ΔNp63 cannot replace the basal gene expression signature, in line with the Notta study where ΔNp63 and other basal cell markers were limited to a smaller subset of basal-like A tumours not associated with poor prognosis. A better understanding of the basal cells may provide critical insights in this matter. Chan-Seng-Yue[5] and Miyabayashi *et al*[62] pointed to the evolution of some classical PDAC into a basal phenotype. One could speculate that tumours arising from or harbouring basal cells would present a wider differentiation potential to transition from classical to basal than those arising from a cell with committed differentiation.

In the light of our discovery of pancreatic basal cells, the established role of basal cells in other tissues and their absence in commonly used mouse experimental models, our observations compel re-interpretation of the cellular pathogenesis of pancreatic diseases.

Author affiliations
[1]Laboratory of Medical and Molecular Oncology, Vrije Universiteit Brussel, Brussel, Belgium
[2]Laboratory of Experimental Gastroenterology, Université Libre de Bruxelles, Bruxelles, Belgium
[3]Hopital Erasme Service de Gastroenterologie d'Hepato-Pancreatologie et d'Oncologie Digestive, Bruxelles, Belgium
[4]Department of Physiological Science, School of Medicine, University of Barcelona (UB), L'Hospitalet de Llobregat, Spain
[5]Pancreas Regeneration: Pancreatic Progenitors and Their Niche Group, Regenerative Medicine Program, P-CMR[C], Institut d'Investigació Biomèdica de Bellvitge - IDIBELL, L'Hospitalet de Llobregat, Spain
[6]Centre de Recherche en Cancérologie de Marseille - CRCM, INSERM UMR1068, CRCM, Marseille, France
[7]COMPO Unit, Centre de Recherche en Cancérologie de Marseille, Marseille, France
[8]Epithelial Carcinogenesis Group, Spanish National Cancer Research Centre, Madrid, Spain
[9]Division of Pediatric General and Thoracic Surgery, University of Pittsburgh Department of Surgery, Pittsburgh, Pennsylvania, USA
[10]Laboratory of Beta Cell Neogenesis, Vrije Universiteit Brussel, Brussel, Belgium
[11]Cell Differentiation Laboratory, Vrije Universiteit Brussel, Brussel, Belgium
[12]Institut de Duve, Université catholique de Louvain, Louvain-la-Neuve, Belgium
[13]Diabetes Research Center, Vrije Universiteit Brussel, Brussel, Belgium
[14]Department of Pathology, Hopital Erasme, Bruxelles, Belgium
[15]Department of Radiation-Oncology, Jules Bordet Institute, Bruxelles, Belgium
[16]Department of Pathology, UZ Brussel, Brussel, Belgium
[17]Department of Pathology, Vrije Universiteit Brussel, Brussel, Belgium

Twitter Abdessamad El Kaoutari @SamadELKA and Meritxell Rovira @TxellRovira

Acknowledgements We would like to thank the Centre for Inflammation Research at VIB-UGent for pancreata of their transgenic mouse model, the Cell Differentiation laboratory for sections of neonatal mice and the use of their antibodies, the Beta Cell Neogenesis laboratory for sections of the PDL mice and the Reproduction and Genetics laboratory for the use of their antibodies. We thank the Beta-Cell Bank and the Central Biobank UZ Brussel for the human samples. Sequencing and analysis were performed by VIB Nucleomics Core (www.nucleomics.be). We thank Suzanne Blotwijk for the advanced statistical analyses.

Contributors This study was conceptualised and designed by SM, KC, MVB, MR and IR. SM, KC, MVB, TA, AFR, JC, AEK, HM, YH, GL, DLDP, ND'H, CB and MR performed experiments, data collection and interpretation. FE, HH, LB, PJ, PiV, ND, J-LVL, WW, PL, FXR and MR provided intellectual input and important samples. SM, KC and IR wrote the manuscript, and all authors edited the manuscript. KC, SM and MVB contributed equally to this paper. JC and AFR contributed equally to this paper as well.

Funding Work in the LMMO laboratory was supported by Stichting tegen Kanker Translational & Clinical Research Grants 2018 #2092. IR is a recipient of an Odysseus I fellowship of the Research Foundation-Flanders (FWO). MVB was financially supported by the Award Cancer Research-Oncology Center Vrije Universiteit Brussel, funded by the bequests of late Ms Esther Desmedt and late Ms Irma Noëand and Wetenschappelijk Fonds Willy Gepts of the UZ Brussel. KC is a recipient of a PhD Fellowship of the FWO (Grant ID 1157221N). Work in the laboratory of FXR is supported, in part, by grant RTI2018-101071-B-I00 from Ministerio de Ciencia e Innovación (Madrid, Spain) (co-funded by the ERDF-EU). CNIO is supported by Ministerio de Ciencia, Innovación y Universidades as a Centro de Excelencia Severo Ochoa SEV-2015-0510. M.R, A.F and J.C reserach was supported by RYC-2017-21950 (AEI/EFS,UE) and SAF2015-73226-JIN (AEI/FEDER, UE). We thank CIBER-BBN and CERCA Programme / Generalitat de Catalunya for IDIBELL institutional support.

Competing interests None declared.

Patient consent for publication Not required.

Ethics approval Mouse experiments in the Cell Differentiation laboratory received ethical approval (16-277-1 (LA1230277)). Ethical approval for the mouse experiments at de Duve institute received under ID 2019/UCL/MD/005. Mouse experiments in the University of Pittsburgh Medical Center received ethical approval under ID 18022411.

Provenance and peer review Not commissioned; externally peer reviewed.

Data availability statement Data are available upon reasonable request. All data relevant to the study are included in the article or uploaded as supplementary information. All relevant data can be requested by contacting the corresponding author.

ORCID iDs
Sandrina Martens http://orcid.org/0000-0003-3421-2581
Katarina Coolens http://orcid.org/0000-0002-3855-512X
Mathias Van Bulck http://orcid.org/0000-0002-5129-8092
Tatjana Arsenijevic http://orcid.org/0000-0002-7261-5587
Abdessamad El Kaoutari http://orcid.org/0000-0003-2334-3121
Hediel Madhloum http://orcid.org/0000-0002-9064-0225
Farzad Esni http://orcid.org/0000-0002-0342-6862
Gunter Leuckx http://orcid.org/0000-0003-2732-397X
Harry Heimberg http://orcid.org/0000-0003-1954-7375
Luc Bouwens http://orcid.org/0000-0001-5767-7002
Patrick Jacquemin http://orcid.org/0000-0002-8781-6453
Diedert Luc De Paep http://orcid.org/0000-0001-8969-6531
Peter in't Veld http://orcid.org/0000-0001-5596-7129
Nicky D'Haene http://orcid.org/0000-0001-8100-377X
Christelle Bouchart http://orcid.org/0000-0003-1714-234X
Nelson Dusetti http://orcid.org/0000-0002-6161-8483
Jean-Luc Van Laethem http://orcid.org/0000-0002-0785-0580
Wim Waelput http://orcid.org/0000-0002-4433-5852
Francisco X Real http://orcid.org/0000-0001-9501-498X
Meritxell Rovira http://orcid.org/0000-0002-0538-4846
Ilse Rooman http://orcid.org/0000-0001-7264-2246

REFERENCES

1 Martens S, Lefesvre P, Nicolle R, *et al*. Different shades of pancreatic ductal adenocarcinoma, different paths towards precision therapeutic applications. *Ann Oncol* 2019;30:1428–36.
2 Bailey P, Chang DK, Nones K, *et al*. Genomic analyses identify molecular subtypes of pancreatic cancer. *Nature* 2016;531:47–52.
3 Somerville TDD, Xu Y, Miyabayashi K, *et al*. TP63-Mediated enhancer reprogramming drives the squamous subtype of pancreatic ductal adenocarcinoma. *Cell Rep* 2018;25:1741–55.
4 Levrero M, De Laurenzi V, Costanzo A. The p53/p63/p73 family of transcription factors: overlapping and distinct functions. *J Cell Sci* 2000;113 (Pt 10:1661–70.
5 Chan-Seng-Yue M, Kim JC, Wilson GW, *et al*. Transcription phenotypes of pancreatic cancer are driven by genomic events during tumor evolution. *Nat Genet* 2020;52:231–40.
6 Goldstein AS, Huang J, Guo C, *et al*. Identification of a cell of origin for human prostate cancer. *Science* 2010;329:568–71.
7 Kim CFB, Jackson EL, Woolfenden AE, *et al*. Identification of bronchioalveolar stem cells in normal lung and lung cancer. *Cell* 2005;121:823–35.

8 Basturk O, Khanani F, Sarkar F, *et al*. DeltaNp63 expression in pancreas and pancreatic neoplasia. *Mod Pathol* 2005;18:1193–8.
9 Di Como CJ, Urist MJ, Babayan I, *et al*. P63 expression profiles in human normal and tumor tissues. *Clin Cancer Res* 2002;8:494–501.
10 Steurer S, Riemann C, Büscheck F, *et al*. P63 expression in human tumors and normal tissues: a tissue microarray study on 10,200 tumors. *Biomark Res* 2021;9.
11 Rock JR, Onaitis MW, Rawlins EL, *et al*. Basal cells as stem cells of the mouse trachea and human airway epithelium. *Proc Natl Acad Sci U S A* 2009;106:12771–5.
12 Mills AA, Zheng B, Wang XJ, *et al*. P63 is a p53 homologue required for limb and epidermal morphogenesis. *Nature* 1999;398:708–13.
13 Yang A, Schweitzer R, Sun D, *et al*. P63 is essential for regenerative proliferation in limb, craniofacial and epithelial development. *Nature* 1999;398:714–8.
14 Blanpain C, Fuchs E. Stem cell plasticity. plasticity of epithelial stem cells in tissue regeneration. *Science* 2014;344:1242281.
15 Gonzales KAU, Fuchs E. Skin and its regenerative powers: an alliance between stem cells and their niche. *Dev Cell* 2017;43:387–401.
16 Pinho AV, Chantrill L, Rooman I. Chronic pancreatitis: a path to pancreatic cancer. *Cancer Lett* 2014;345:203–9.
17 Matsumoto K, Mitani TT, Horiguchi SA, *et al*. Advanced cubic tissue clearing for whole-organ cell profiling. *Nat Protoc* 2019;14:3506–37.
18 Zhao S, Todorov MI, Cai R, *et al*. Cellular and molecular probing of intact human organs. *Cell* 2020;180:796–812.
19 Ueda HR, Ertürk A, Chung K, *et al*. Tissue clearing and its applications in neuroscience. *Nat Rev Neurosci* 2020;21:61–79.
20 Kloesch B, Ionasz V, Paliwal S, *et al*. A GATA6-centred gene regulatory network involving HNFs and ΔNp63 controls plasticity and immune escape in pancreatic cancer. *Gut* 2021;Apr. doi:10.1136/gutjnl-2020-321397. [Epub ahead of print: 12 Apr 2021].
21 Nicolle R, Gayet O, Duconseil P, *et al*. A transcriptomic signature to predict adjuvant gemcitabine sensitivity in pancreatic adenocarcinoma. *Ann Oncol* 2021;32:250–60.
22 Nicolle R, Blum Y, Duconseil P, *et al*. Establishment of a pancreatic adenocarcinoma molecular gradient (PAMG) that predicts the clinical outcome of pancreatic cancer. *EBioMedicine* 2020;57:102858.
23 Strobel O, Rosow DE, Rakhlin EY, *et al*. Pancreatic duct glands are distinct ductal compartments that react to chronic injury and mediate Shh-induced metaplasia. *Gastroenterology* 2010;138:1166–77.
24 Zhang D, Park D, Zhong Y, *et al*. Stem cell and neurogenic gene-expression profiles link prostate basal cells to aggressive prostate cancer. *Nat Commun* 2016;7:10798.
25 Hackett NR, Shaykhiev R, Walters MS, *et al*. The human airway epithelial basal cell transcriptome. *PLoS One* 2011;6:e18378.
26 Yeung CH, Nashan D, Sorg C, *et al*. Basal cells of the human epididymis--antigenic and ultrastructural similarities to tissue-fixed macrophages. *Biol Reprod* 1994;50:917–26.
27 Mosunjac MB, Lewis MM, Lawson D, *et al*. Use of a novel marker, calponin, for myoepithelial cells in fine-needle aspirates of papillary breast lesions. *Diagn Cytopathol* 2000;23:151–5.
28 Lapi E, Iovino A, Fontemaggi G, *et al*. S100A2 gene is a direct transcriptional target of p53 homologues during keratinocyte differentiation. *Oncogene* 2006;25:3628–37.
29 May R, Sureban SM, Lightfoot SA, *et al*. Identification of a novel putative pancreatic stem/progenitor cell marker DCAMKL-1 in normal mouse pancreas. *Am J Physiol Gastrointest Liver Physiol* 2010;299:G303–10.
30 van der Flier LG, Haegebarth A, Stange DE, *et al*. OLFM4 is a robust marker for stem cells in human intestine and marks a subset of colorectal cancer cells. *Gastroenterology* 2009;137:15–17.
31 Kelly OG, Chan MY, Martinson LA, *et al*. Cell-Surface markers for the isolation of pancreatic cell types derived from human embryonic stem cells. *Nat Biotechnol* 2011;29:750–6.
32 Bailey JM, Alsina J, Rasheed ZA, *et al*. Dclk1 marks a morphologically distinct subpopulation of cells with stem cell properties in preinvasive pancreatic cancer. *Gastroenterology* 2014;146:245–56.
33 Westphalen CB, Takemoto Y, Tanaka T, *et al*. Dclk1 defines quiescent pancreatic progenitors that promote injury-induced regeneration and tumorigenesis. *Cell Stem Cell* 2016;18:441–55.
34 Ahmad S, Ahmad A. Chapter 6 - epithelial regeneration and lung stem cells. In: Sidhaye VK, ed. *Lung epithelial biology in the pathogenesis of pulmonary disease. Koval MBT-LEB in the P of PD*. Boston: Academic Press, 2017: 91–102. https://www.sciencedirect.com/science/article/pii/B9780128038093000063
35 Messal HA, Alt S, Ferreira RMM, *et al*. Tissue curvature and apicobasal mechanical tension imbalance instruct cancer morphogenesis. *Nature* 2019;566:126–30.
36 Li W, Germain RN, Gerner MY. Multiplex, quantitativ$_e$ cellular analysis in larg$_e$ tissu$_e$ volumes with clearing-enhanced 3D microscopy (C$_e$3D). *Proc Natl Acad Sci U S A* 2017;114:E7321–30.
37 Martinelli P, Real FX. *Animal modeling of pancreatitis-to-cancer progression*. New York: Springer, 2017: 313–47.
38 Gong S, Zheng C, Doughty ML, *et al*. A gene expression atlas of the central nervous system based on bacterial artificial chromosomes. *Nature* 2003;425:917–25.
39 Furukawa T, Duguid WP, Rosenberg L, *et al*. Long-Term culture and immortalization of epithelial cells from normal adult human pancreatic ducts transfected by the E6E7 gene of human papilloma virus 16. *Am J Pathol* 1996;148:1763–70.
40 Backx E, Wauters E, Baldan J, *et al*. Mecom permits pancreatic acinar cell dedifferentiation avoiding cell death under stress conditions. *Cell Death Differ* 2021. doi:10.1038/s41418-021-00771-6. [Epub ahead of print: 24 Mar 2021].
41 Cebola I, Rodríguez-Seguí SA, Cho CH-H, *et al*. Tead and YAP regulate the enhancer network of human embryonic pancreatic progenitors. *Nat Cell Biol* 2015;17:615–26.
42 Zhao R, Fallon TR, Saladi SV, *et al*. Yap tunes airway epithelial size and architecture by regulating the identity, maintenance, and self-renewal of stem cells. *Dev Cell* 2014;30:151–65.
43 Rock JR, Randell SH, Hogan BLM. Airway basal stem cells: a perspective on their roles in epithelial homeostasis and remodeling. *Dis Model Mech* 2010;3:545–56.
44 Real FX, Vilá MR, Skoudy A, *et al*. Intermediate filaments as differentiation markers of exocrine pancreas. II. expression of cytokeratins of complex and stratified epithelia in normal pancreas and in pancreas cancer. *Int J Cancer* 1993;54:720–7.
45 Kern HF. Fine structure of the human exocrine pancreas. In: *The pancreas: biology, pathobiology, and disease*. 2nd ed. New York: Raven Press, 1993: 9–19.
46 Madden ME, Sarras MP. The pancreatic ductal system of the rat. *Pancreas* 1989;4:472–85.
47 Schwenk J, Makovitzky J. Tissue expression of the cancer-associated antigens Ca 19-9 and CA-50 in chronic pancreatitis and pancreatic carcinoma. *Int J Pancreatol* 1989;5:85–95.
48 Qadir MMF, Álvarez-Cubela S, Klein D, *et al*. Single-Cell resolution analysis of the human pancreatic ductal progenitor cell niche. *Proc Natl Acad Sci U S A* 2020;117:10876–87.
49 Muraro MJ, Dharmadhikari G, Grün D, *et al*. A single-cell transcriptome atlas of the human pancreas. *Cell Syst* 2016;3:385–94.
50 Enge M, Arda HE, Mignardi M, *et al*. Single-Cell analysis of human pancreas reveals transcriptional signatures of aging and somatic mutation patterns. *Cell* 2017;171:321–30.
51 Segerstolpe Åsa, Palasantza A, Eliasson P, *et al*. Single-Cell transcriptome profiling of human pancreatic islets in health and type 2 diabetes. *Cell Metab* 2016;24:593–607.
52 Kwon O-J, Zhang L, Ittmann MM, *et al*. Prostatic inflammation enhances basal-to-luminal differentiation and accelerates initiation of prostate cancer with a basal cell origin. *Proc Natl Acad Sci U S A* 2014;111:E592–600.
53 Paul MK, Bisht B, Darmawan DO, *et al*. Dynamic changes in intracellular ROS levels regulate airway basal stem cell homeostasis through Nrf2-dependent Notch signaling. *Cell Stem Cell* 2014;15:199–214.
54 Kopp JL, Grompe M, Sander M. Stem cells versus plasticity in liver and pancreas regeneration. *Nat Cell Biol* 2016;18:238–45.
55 Dekoninck S, Blanpain C, dynamics Scell. Stem cell dynamics, migration and plasticity during wound healing. *Nat Cell Biol* 2019;21:18–24.
56 Dirice E, De Jesus DF, Kahraman S, *et al*. Human duct cells contribute to β cell compensation in insulin resistance. *JCI Insight* 2019;4. doi:10.1172/jci.insight.99576. [Epub ahead of print: 18 04 2019].
57 Hosokawa S, Furuyama K, Horiguchi M, *et al*. Impact of SOX9 dosage and Hes1-mediated Notch signaling in controlling the plasticity of adult pancreatic duct cells in mice. *Sci Rep* 2015;5:8518.
58 Krah NM, Murtaugh LC, Differentiation MLC. Differentiation and Inflammation: 'Best Enemies' in Gastrointestinal Carcinogenesis. *Trends Cancer* 2016;2:723–35.
59 Espinet E, Gu Z, Imbusch CD, *et al*. Aggressive PDACs show hypomethylation of repetitive elements and the execution of an intrinsic IFN program linked to a ductal cell of origin. *Cancer Discov* 2021;11:638–59.
60 Flowers BM, Xu H, Mulligan AS, *et al*. Cell of origin influences pancreatic cancer subtype. *Cancer Discov* 2021;11:660–77.
61 Grimont A, Pinho AV, Cowley MJ, *et al*. Sox9 regulates ErbB signalling in pancreatic cancer development. *Gut* 2015;64:1790–9.
62 Miyabayashi K, Baker LA, Deschênes A, *et al*. Intraductal transplantation models of human pancreatic ductal adenocarcinoma reveal progressive transition of molecular subtypes. *Cancer Discov* 2020;10:CD-20-0133.

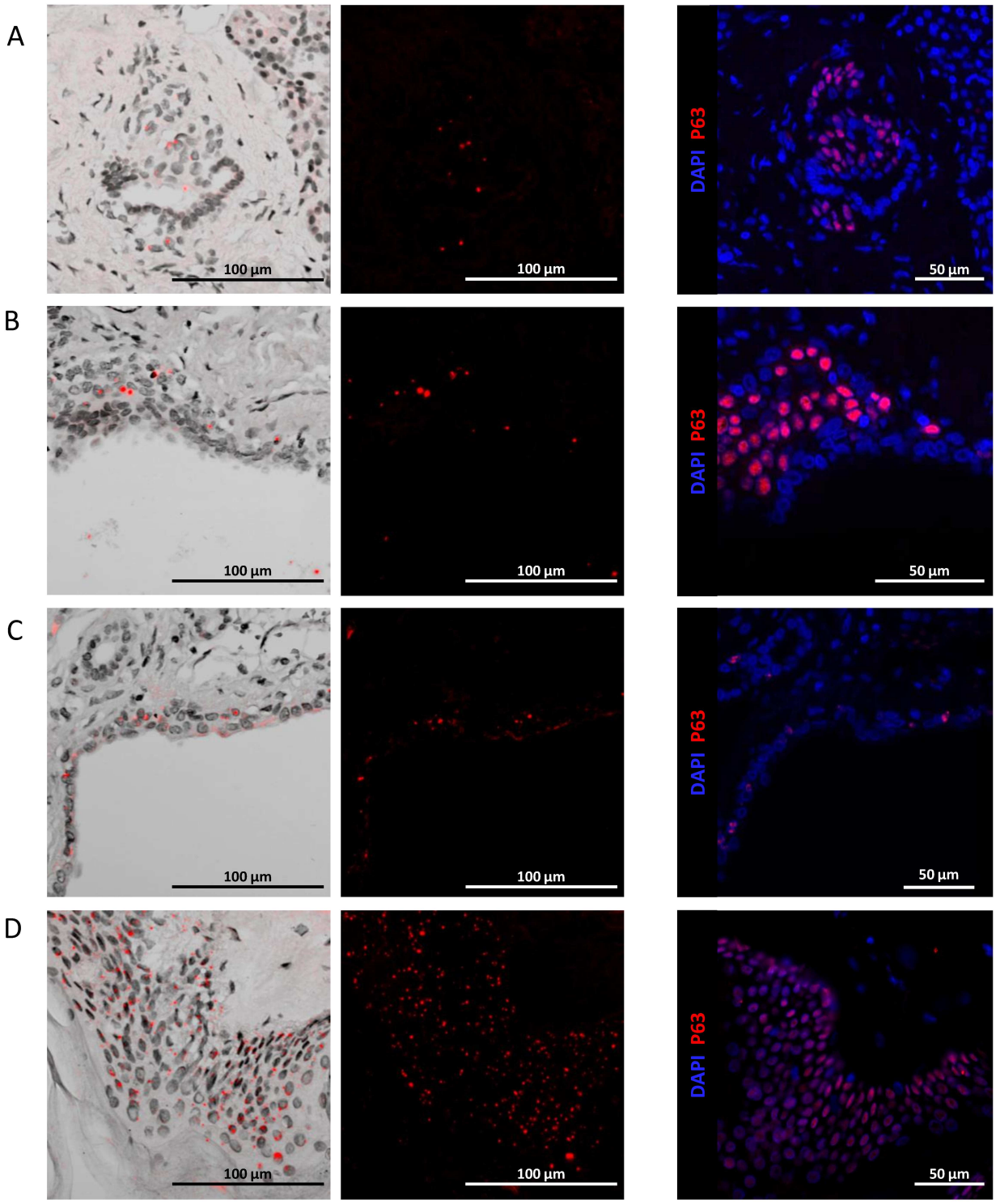
A
100 µm
100 µm
DAPI P63
50 µm
B
100 µm
100 µm
DAPI P63
50 µm
C
100 µm
100 µm
DAPI P63
50 µm
D
100 µm
100 µm
DAPI P63
50 µm

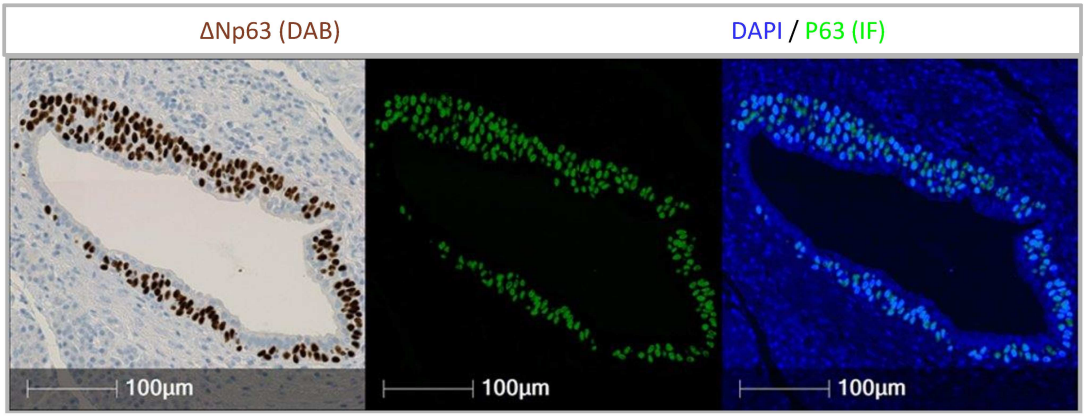
E
ΔNp63 (DAB)
DAPI / P63 (IF)
100µm
100µm
100µm

S Figure 1: RNA detection of ΔNp63 using BaseScope RNA *in situ* hybridization. (A-C) RNA detection in healthy donor pancreas (A), chronic pancreatitis (B) and normal tissue adjacent to PDAC area (C), with the corresponding P63 staining below. RNA is visualized as red dots. (D) RNA detection in positive control tissue (human skin). (E) Validation of P63 antibody in immunofluorescence (IF) on the right with ΔNp63 antibody staining in immunohistochemistry (IHC) on the left.

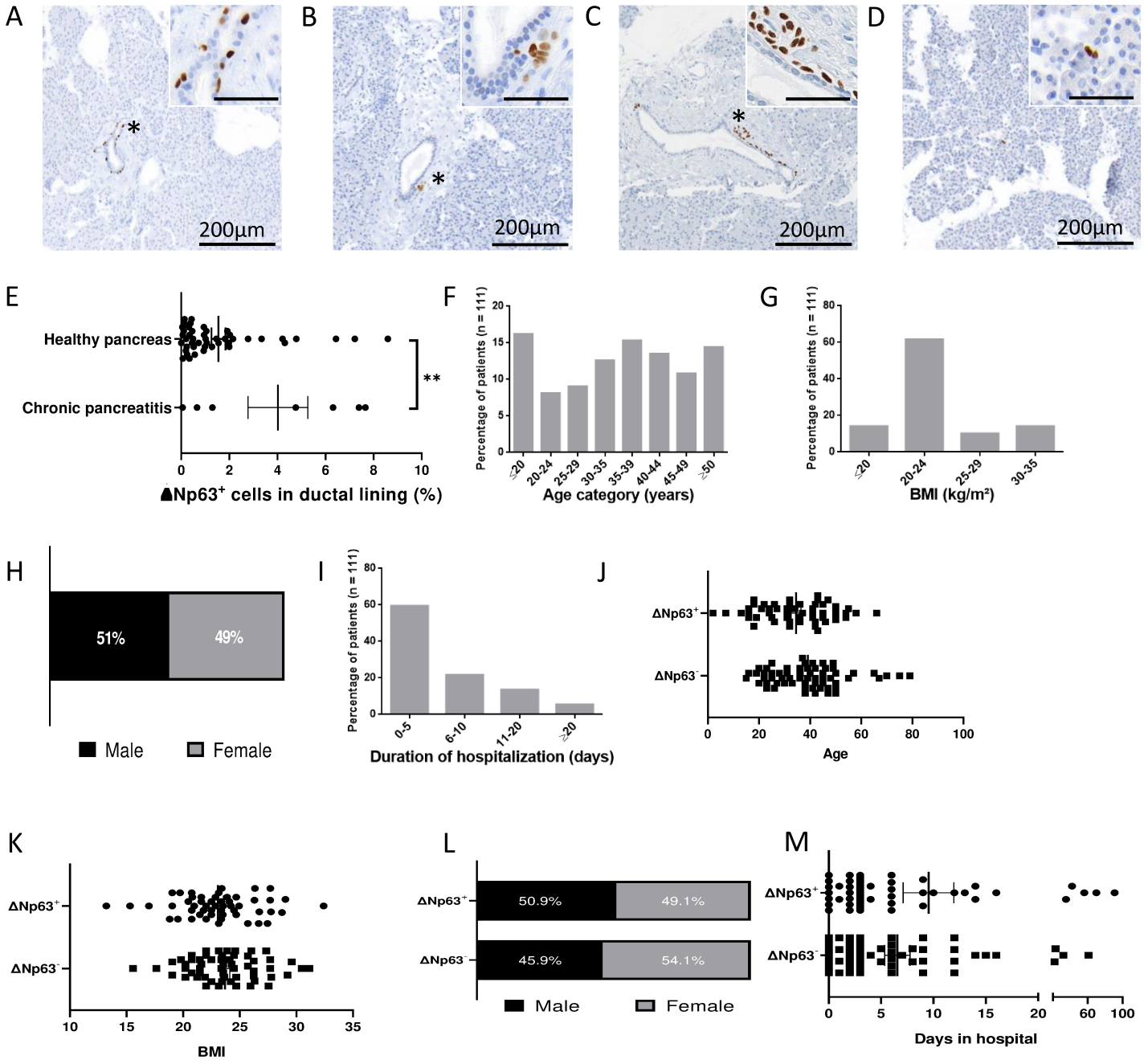

S Figure 2: (A-D) Location of ΔNp63⁺ cells throughout a healthy pancreas: (A) Cells can be located basally within a duct, (B) they can form a small cluster near a duct or (C) there can be both groups and single cells combined. (D) ΔNp63⁺ cells can rarely be found within acinar tissue. Scale bars indicate 200µm, scale bars on insets are 50 µm. (E) Percentage of cells within the ductal lining in normal pancreas (n=46) and chronic pancreatitis (n=7) (**p=0,044) Characteristics of all normal human pancreas donors with ΔNp63 detected in a section (n=53): (F) Age, (G) Gender, (H) Days spent in the intensive care unit, (I). Characteristics of all human pancreas donors with ΔNp63 detected in a section (n=53) and without ΔNp63 detected in a section (n=61). (J) Age, (K) Gender, (L) Days spent in the intensive care unit and (M) BMI.

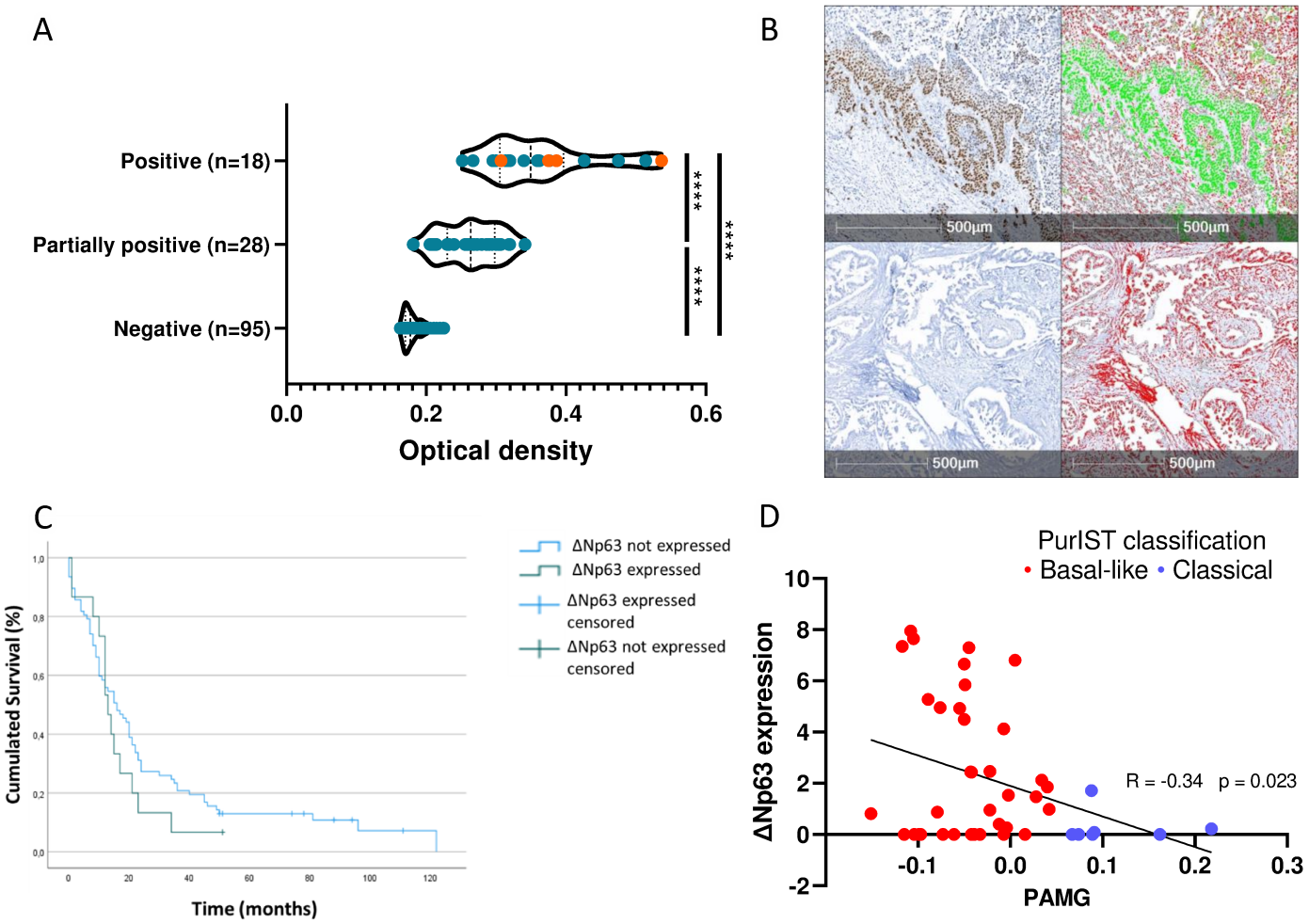

S Figure 3: ΔNp63 expression in pancreatic ductal adenocarcinoma samples. (A-B) Quantification of ΔNp63 expression displayed as optical density for four different groups of tumours (n=141), lacking ΔNp63 (negative), only in a few cells (partially positive) and samples that express ΔNp63 (positive). Four adenosquamous samples, which all fall in the positive group, are indicated in orange. Mean ± SEM is shown. ****p<0,001 (B) Visualization of the quantification through image analysis (HALO). IHC stainings are quantified in red (haematoxylin) and green (ΔNp63). (C) Cumulated survival in patients with PDAC with and without ΔNp63 expression (n=92 with data available). (D) Negative correlation between ΔNp63 and the PAMG score in PDAC cell lines (n=44).

A

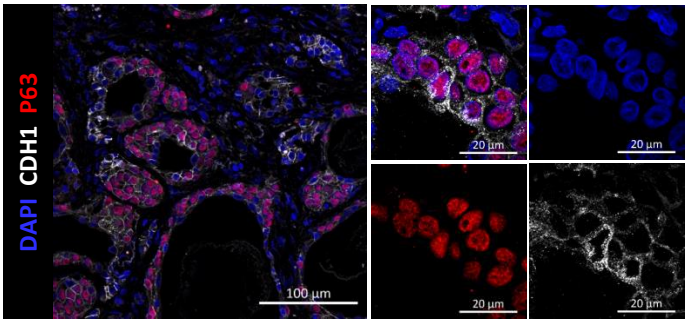

S Figure 4: **ΔNp63⁺ cells are epithelial cells.** IF for E-cadherin (white) and P63 (red).

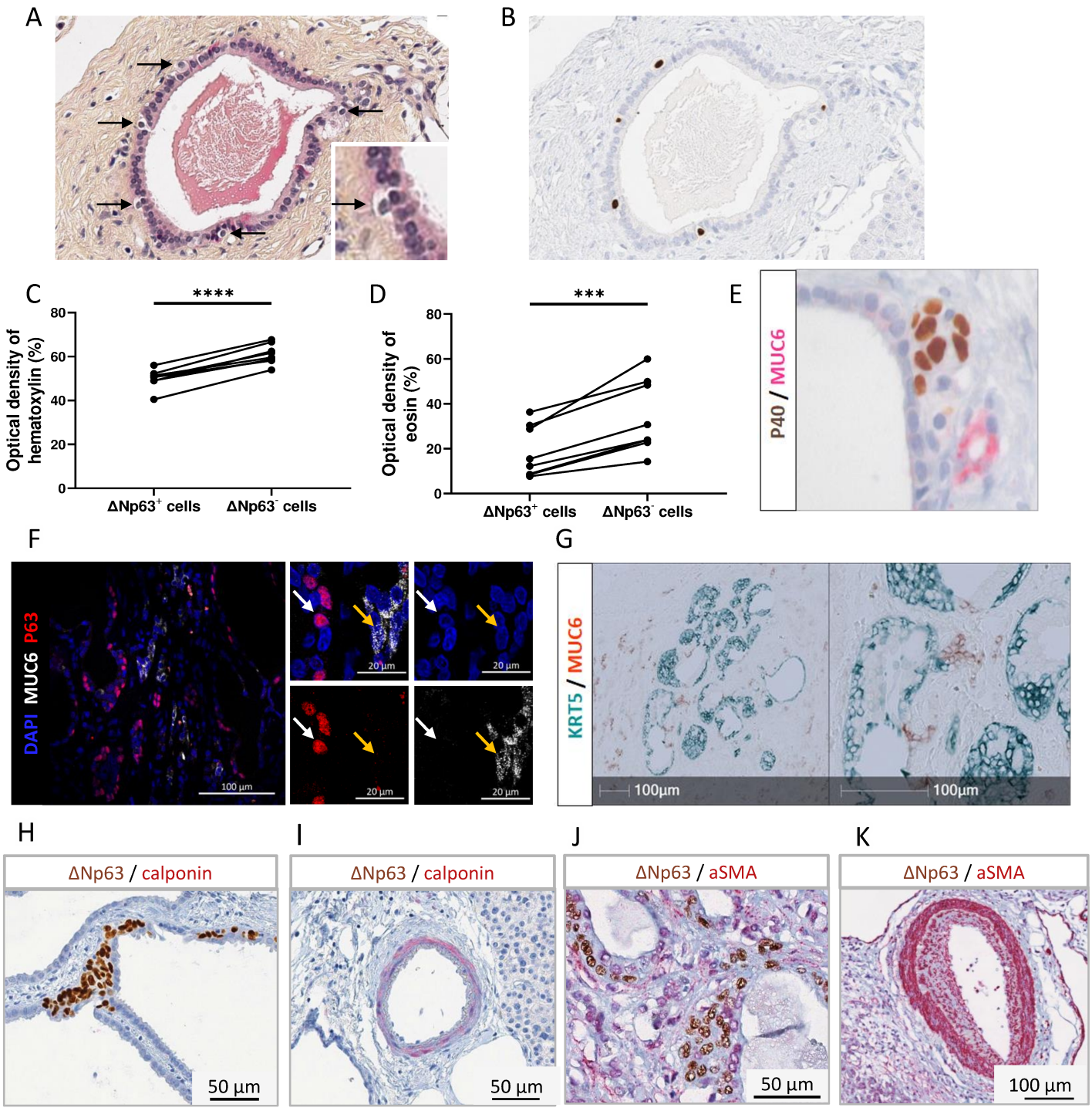

S Figure 5: (A) HES staining of a duct in a human healthy pancreas. Inset on the right bottom shows magnification of one ΔNp63⁺ cell. Black arrows point to ΔNp63⁺ cells. (B) Consecutive section of A showing IHC staining for ΔNp63. Quantification of the (C) haematoxylin and (D) eosin positivity in ΔNp63 cells compared to ductal cells (n=8). One line indicates one slide that was analysed for both ΔNp63⁺ and ΔNp63⁻ cells. (***p< 0,001; ****p< 0,0001). (E) IHC for ΔNp63 (brown) and MUC6 (red). (F) IF for P63 (red) and MUC6 (white). White arrow indicates ΔNp63⁺ cell, the orange arrow indicates a MUC6⁺ cell. (G) IHC staining for KRT5 (green) and MUC6 (red). (H) IHC for ΔNp63 (brown) and calponin (red) in a duct positive for ΔNp63. (I) shows positive control for calponin in the wall of a blood vessel. (J) IHC staining for ΔNp63 (brown) and aSMA (red) in a duct positive for ΔNp63. (K) shows positive control for aSMA.

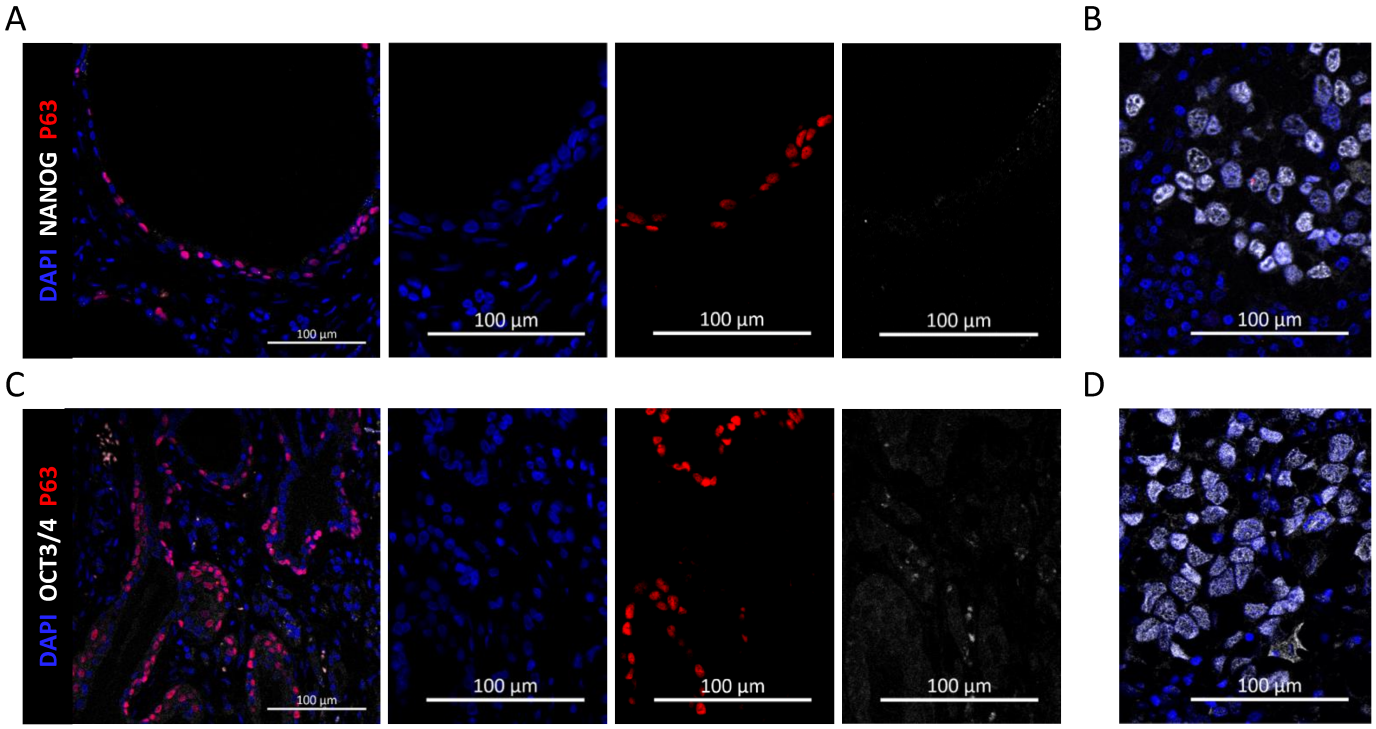

S Figure 6: **ΔNp63⁺ cells do not express typical pluripotent stem cell markers.** (A) IF for P63 (red) and NANOG (white). (B) Positive expression of NANOG is shown in a seminoma in panel. (C) IF for P63 (red) and OCT4 (white). (D) Positive expression of OCT4 is shown in a seminoma in panel.

A

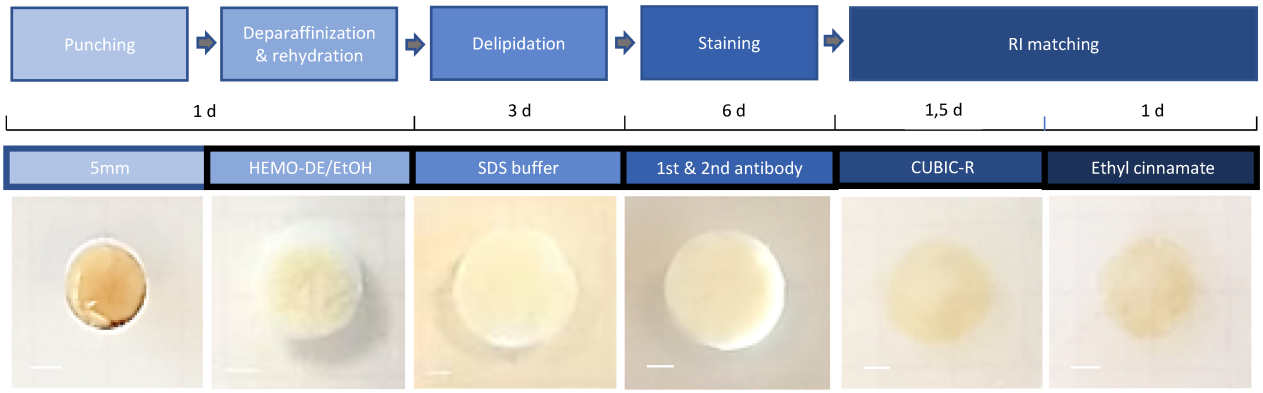

B

Protocol	Delipidation	RI matching	Duration	High resolution imaging
Modified IDISCO[19]	dichloromethane/methanol	dibenzyl ether (DBE)	20 days	confocal microscopy
FLIP-IT	SDS buffer	CUBIC-R/Ethyl Cinnamate(Eci)	13 days	Lightsheet miscroscopy

C

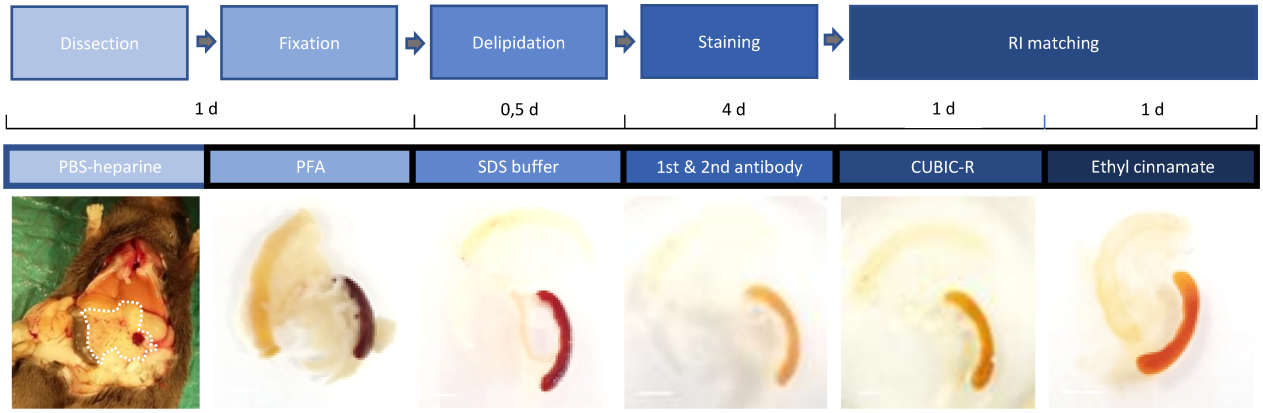

D

Protocol	Delipidation	RI matching	Duration	High resolution imaging
FLASH[35]	SDS/boric acid	Methyl Salicylate	7 days	confocal microscopy
FLIP-IT	SDS buffer	CUBIC-R/Ethyl Cinnamate(Eci)	8 days	Lightsheet miscroscopy

S Figure 7: FLIP-IT overview of human and mouse sample processing. (A) FLIP-IT protocol steps in archival FFPE human samples and representative pictures of the samples. Scale bars correspond to 2mm. (B) Table comparing key protocol steps for 3D human pancreas sample processing workflow. (C) FLIP-IT in fresh PFA-fixed mouse samples and representative pictures of the samples. Scale bars correspond to 5mm. (D) Table comparing key protocol steps for whole mouse pancreas sample processing workflow.

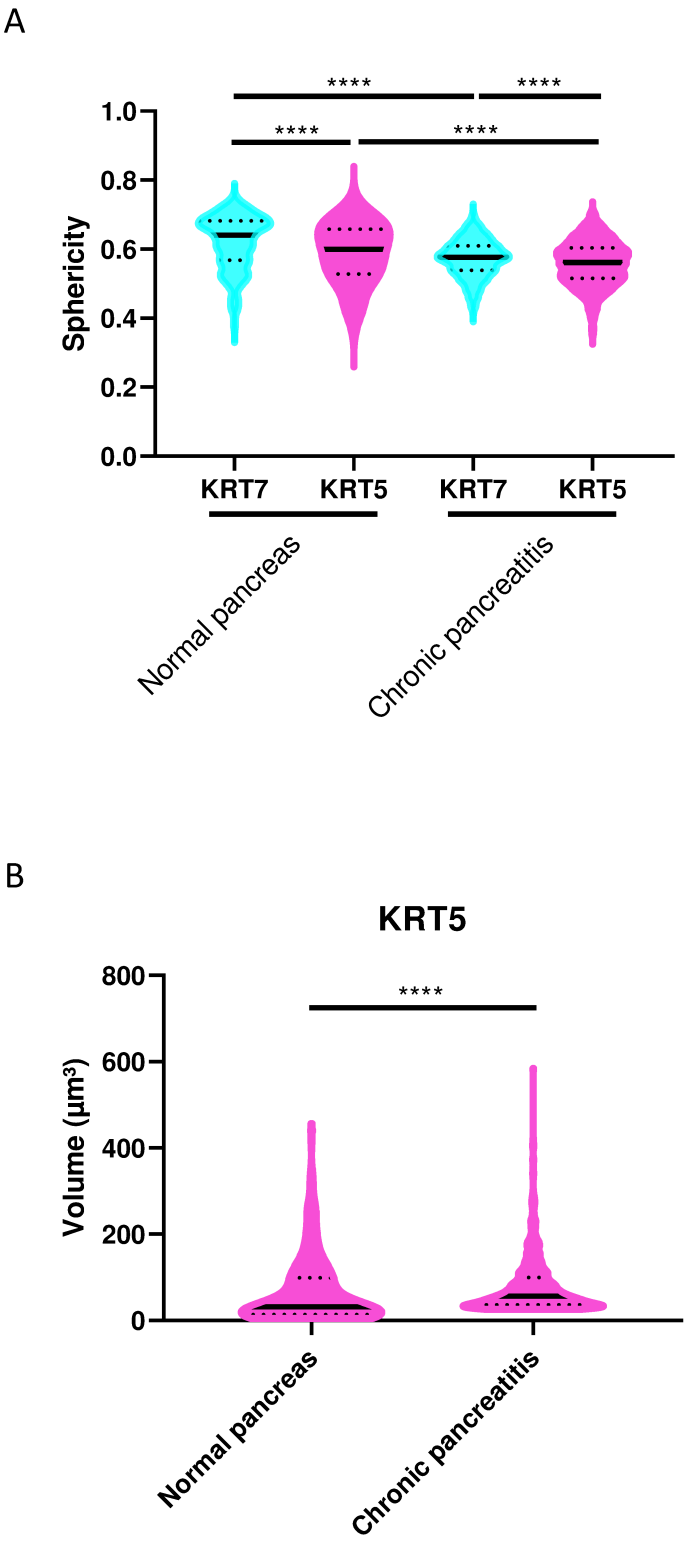

S Figure 8: KRT5⁺ cell sphericity and volume changes in chronic pancreatitis compared to normal human pancreas. (A) Sphericity quantification of KRT5⁺ and KRT7⁺ cells in both normal human pancreas and chronic pancreatitis. (B) Volume quantification of KRT5⁺ cells in both normal human pancreas and chronic pancreatitis. (****p< 0,0001; n=1; >250 cells counted per group.)

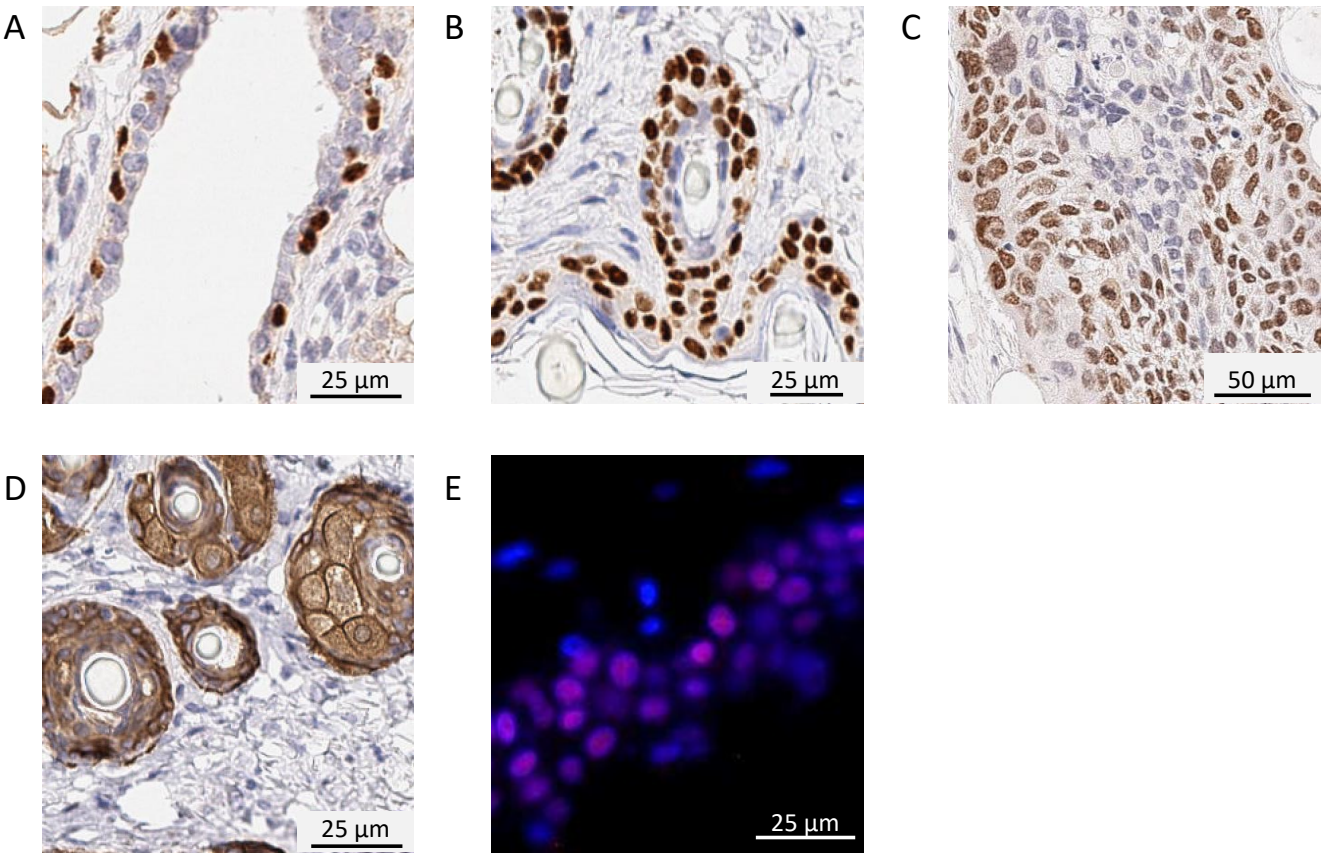

S Figure 9: The ΔNp63 and KRT14 antibodies showed strong positivity in positive control mouse tissues. (A) ΔNp63 IHC staining in a healthy mouse mammary gland, staining the myo-epithelial cells. (B) ΔNp63 IHC staining in healthy mouse skin, staining nuclei in the epidermis. (C) ΔNp63 IHC staining in a human adenosquamous tumour. (D) KRT14 IHC staining in the hair follicles of a human skin section. (E) P63 IF staining of nuclei of the basal cells in the epidermis of human skin.

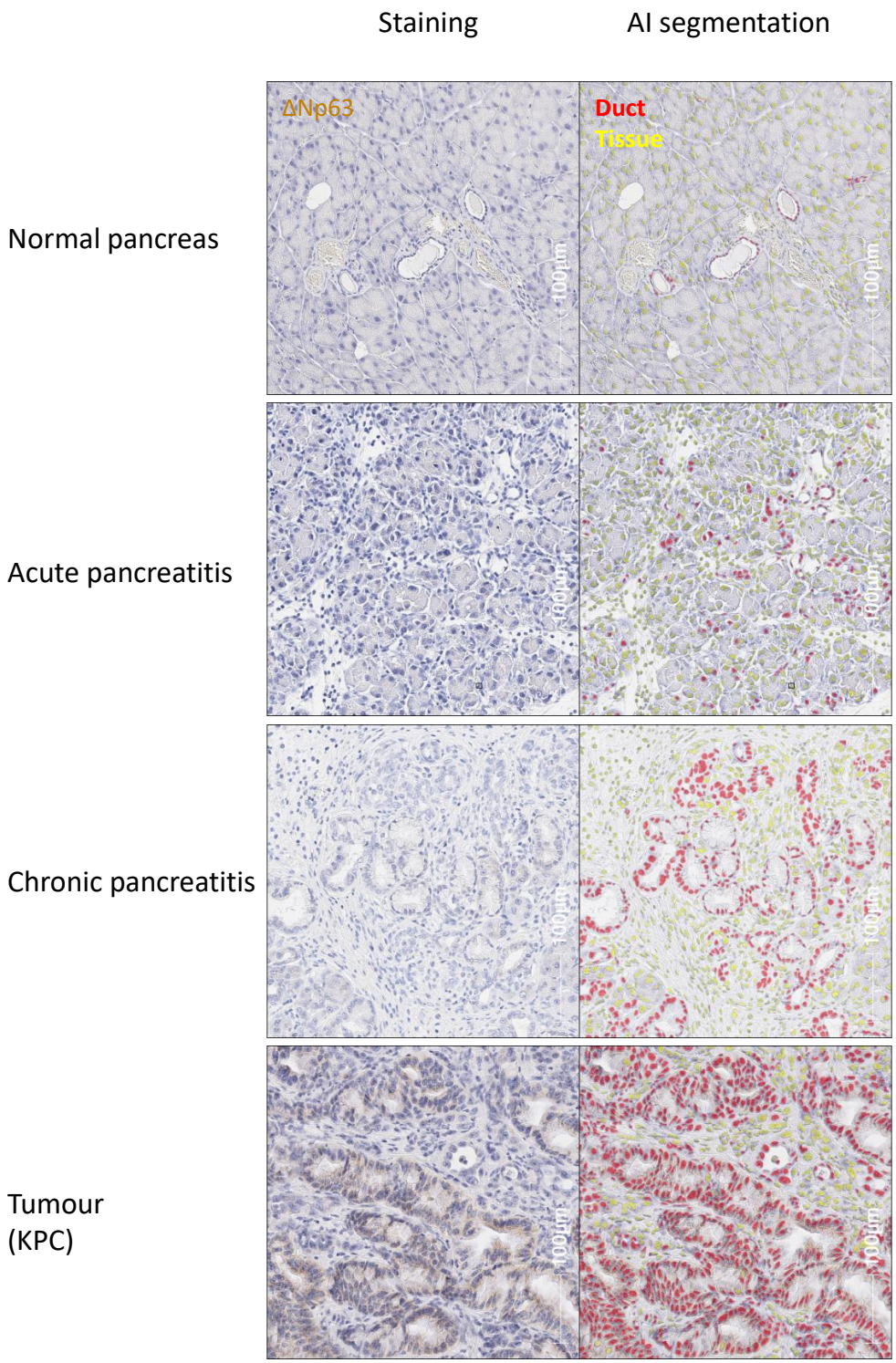

S Figure 10: ΔNp63⁺ are not found in healthy or diseased murine pancreas. Representative images of normal mouse pancreas, acute pancreatitis, chronic pancreatitis and KPC tumour model do not show staining for ΔNp63. AI segmentation shows ductal (red) and tissue cells (yellow). None of the segmented cells shows ΔNp63 positivity. n>71

A

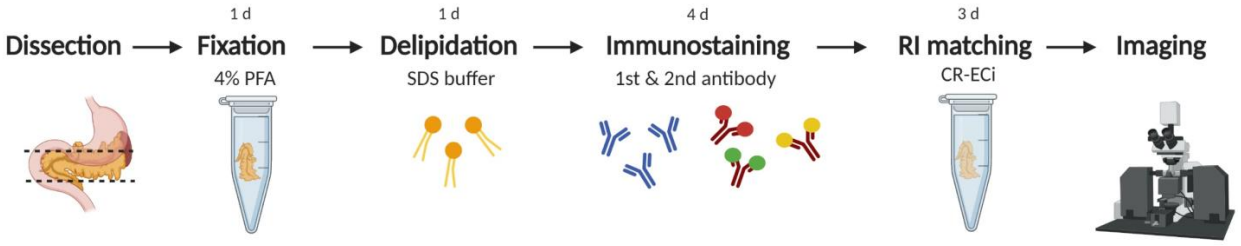
Dissection
1 d
Fixation
4% PFA
1 d
Delipidation
SDS buffer
4 d
Immunostaining
1st & 2nd antibody
3 d
RI matching
CR-ECi
Imaging

B

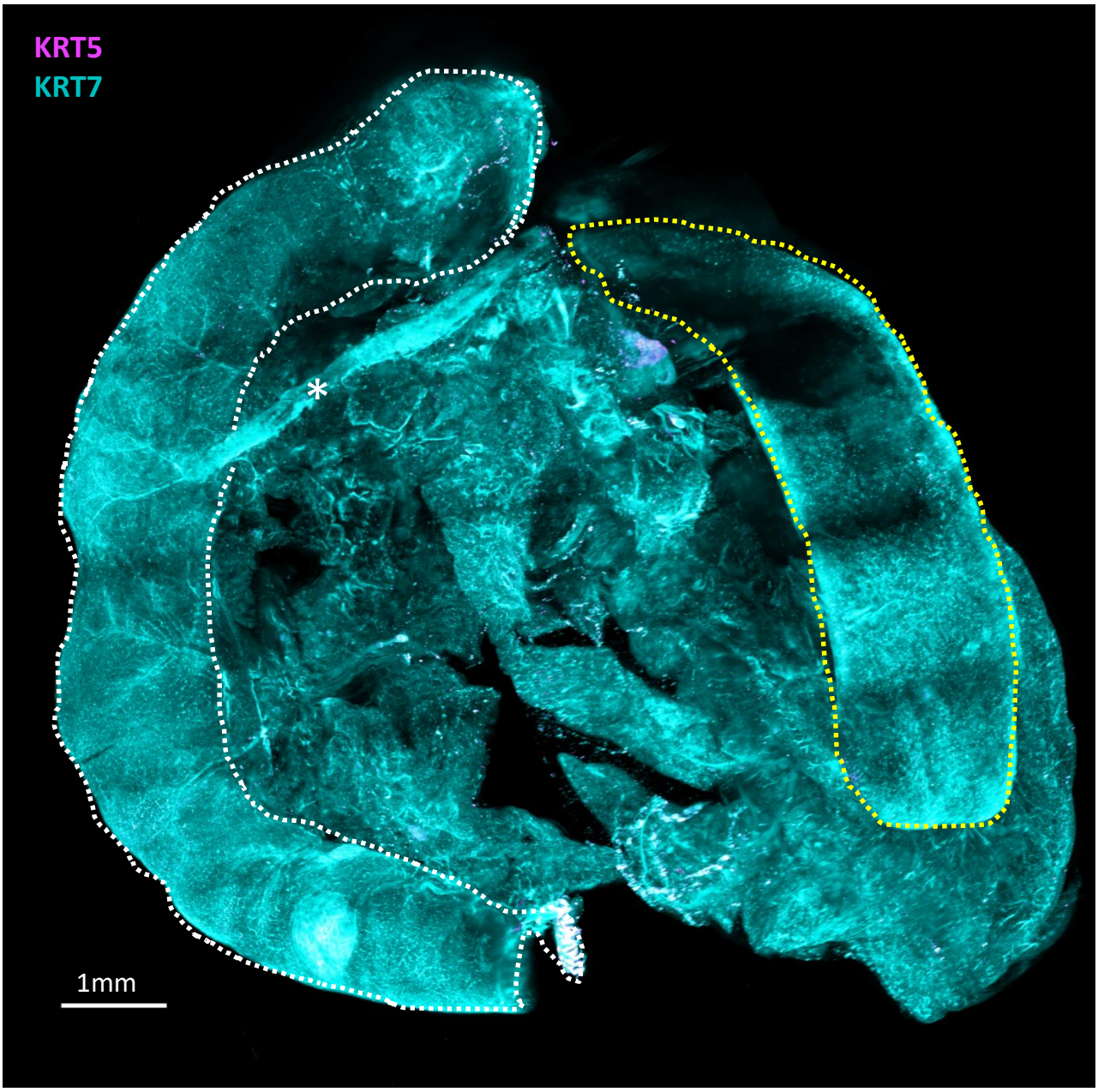
KRT5
KRT7
1mm

S Figure 11: FLIP-IT applied to whole mouse pancreas and attached duodenum and spleen. (A) Processing protocol of fresh mouse samples. (B) Overview 3D rendering of normal mouse pancreas stained for KRT5 (pink) and KRT7 (cyan). No KRT5^{+} were seen in the mouse pancreas. Some pink color is present in areas showing nonspecific staining (confirmed at higher magnification). Asterisk shows large duct. White dotted line shows duodenum. Yellow dotted line shows spleen. Objective 5x, zoom 0.36 . Scale bar corresponds to 1mm. n=3

A

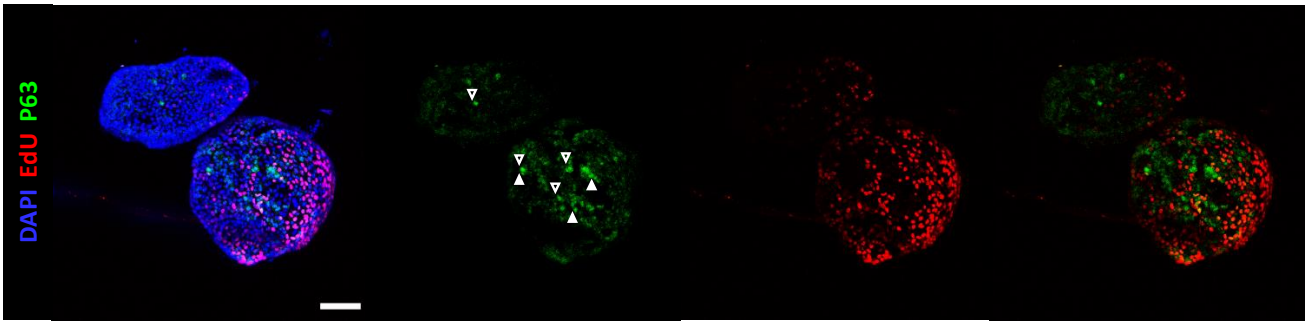

S Figure 12: IF staining for ΔNp63 (green) and EdU (red). Nuclei are stained blue (DAPI). White arrowheads indicate $p63^+$ EdU^+ cells, whereas non-filled arrowheads indicate $P63^+$, EdU^- cells. Scale bar indicates 100 µm.

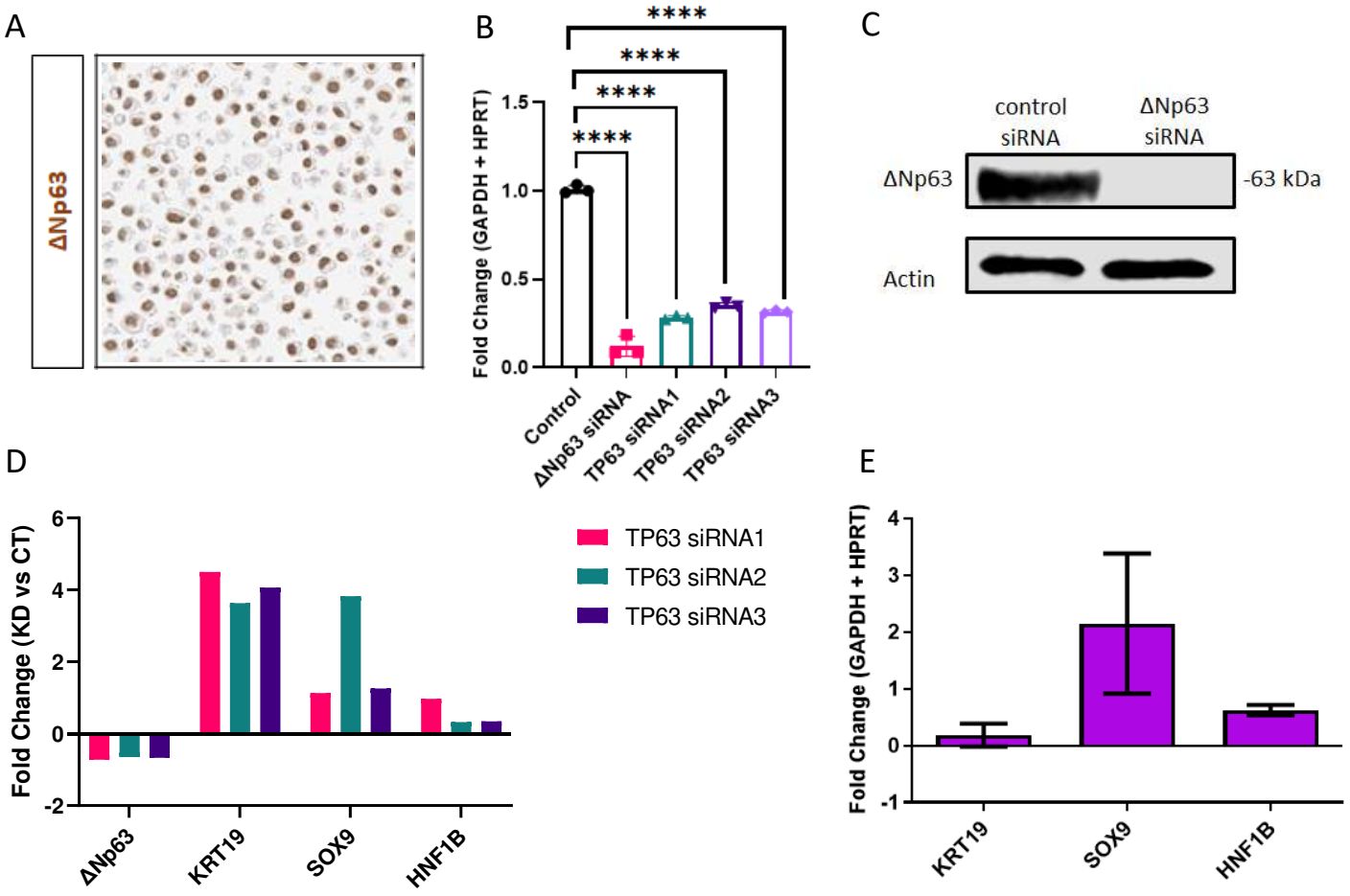

S Figure 13: Confirmation and validation of (ΔN)P63 knockdown. (A) IHC staining for ΔNp63 in HPDE cells. (B) Validation of other *TP63* siRNA's (****p< 0,0001). (C) Western blot for ΔNp63 and β-actin. (D) qRT-PCR for *ΔNp63, KRT19, SOX9* and *HNF1B*. (E) qRT-PCR analysis for *Krt19, Sox9* and *Hnf1b* in organoids derived from medium sized ducts.

SUPPLEMENTARY MATERIALS AND METHODS

Human samples

Human samples (FFPE embedded tissue blocks and their donor characteristics) were collected from deceased multi organ donors by the Beta-cell bank UZ Brussels, as part of their clinical islet transplantation program. Pancreata of Whipple resections, chronic pancreatitis and autopsy samples plus patient characteristics were obtained from the department of Anatomopathology of UZ Brussels. The study included FFPE pancreatic cancer tissue blocks selected from the Anatomopathology department of Erasme Hospital (ULB-Brussels). Ethical consent was given by the Committee of Medical Ethics - UZ Brussels and samples were obtained through the Central Biobank UZ Brussel (17-183) and partner biobank at Erasme Hospital (B2020/001).

Mouse samples

Mice were sacrificed in accordance with institutional ethical guidelines and regulations and were approved by VUB Animal Ethics Committee (ethical approval 19-595-3). Mouse experiments in the Cell Differentiation lab received ethical approval (16-277-1 (LA1230277)). Ethical approval for the mouse experiments at de Duve institute received ID 2019/UCL/MD/005. Mouse experiments in the University of Pittsburgh Medical Centre received ethical approval under ID 18022411.

Haematoxylin-eosin Saffron staining

After baking, deparaffinization and rehydration, sections were stained with haematoxylin (Sigma-Aldrich, St-Louis, MO, USA) for 5 minutes and were then differentiated with alcoholic acid and were blued in lithium carbonate. The slides were then stained with Erythrosine B (Sigma-Aldrich) for 2 minutes and 30 seconds. Slides were dehydrated in propanol and were then stained with saffron for 30 seconds and mounted with Pertex mounting medium.

Immunohistochemistry

For singleplex ΔNp63 stainings on human samples, the automated stainer Ventana Benchmark ULTRA was used with the anti-p40 antibody, clone BC28 (790-4950, Roche, Switzerland). For brightfield duplex stainings, the Benchmark ULTRA was used with the anti-p40 antibody in combination with the anti-CA19.9 antibody (760-2609, Roche) and the anti-MUC6 antibody (760-4390, Roche).

On mouse pancreas, we performed manual DAB stainings as the automated stainer detects all mouse IgGs. One to three random sections were assessed per block. Sections were baked, deparaffinised and rehydrated. Endogenous peroxidase activity was blocked using 3% Hydrogen Peroxidase in methanol for 30 minutes. Antigen retrieval was performed using citrate buffer (Sigma-Aldrich) in a pressure cooker for 40 minutes, and protein block was done using casein block (Thermo Fisher Scientific, Waltham, Massachusetts, USA) concentrated 25%. The primary antibody was incubated overnight at 4°C. The antibodies anti-p40 (ab167612, Abcam, Cambridge, UK; diluted 1/200), anti-p40 (ABS552, Sigma-Aldrich; diluted 1/50.000), anti-KRT14 (1/2000, HPA023040, Atlas antibodies, Bromma, Sweden) or anti-KRT5 (1/200, ab52635, Abcam) were used, which gave identical results. The next day, slides were incubated for 30 minutes with biotinylated goat anti-rabbit IgG antibody (Vector, Burlingame, California, USA, BA-1000, 1/200). Afterwards, slides were incubated for 30 minutes with a Streptavidin-biotin-HRP complex (VECTASTAIN(R) ELITE(R) ABC HRP Detection Kit, Vector). DAB incubation was done by diluting DAB concentrate 10 times in peroxide buffer (11718096001, Roche), after which slides were counterstained with haematoxylin for 30 seconds, differentiated in alcoholic acid and blued in

lithium carbonate. Slides were dehydrated and mounted with Pertex mounting medium. For these stainings, a positive control of either a mouse mammary gland or mouse skin were included.

For multiplex IHC staining the same protocol as above was followed however with minor modifications. On the second day Ultrabrite IHC Red Chromogen (BioVision, Milpitas, California, USA) was used instead of DAB. Afterwards, casein blocking was performed again and slides were incubated overnight at 4°C with the second primary antibody. On day three, UltraBrite IHC green chromogen (BioVision) was used. Slides were rinsed, air-dried and mounted with Pertex mounting medium.

For immunofluorescence (IF), we resorted to a P63 antibody (ab735, Abcam) as the ΔNp63 antibodies mentioned before, and additionally anti-p40 (ab172731, Abcam) were not suitable for multiplex IF. Slides were processed as above and incubated overnight at 4°C with a cocktail of antibodies, always including the P63 antibody (1/50). Other primary antibodies used were E-cadherin (1/100, AB5733, Sigma-Aldrich), KRT19 (1/100, TROMA-III, obtained from the Developmental Studies Hybridoma Bank, created by the NICHD of the NIH and maintained at The University of Iowa, Department of Biology, Iowa City, IA 52242), SOX9 (1/1000, ABE2868, Sigma-Aldrich), HNF1β (1/100, sc-7411, Santa Cruz, Dallas, Texas, USA), PDX1 (1/100, AF2419, RandD), KRT5 (1/100, ab52635, Abcam), KRT14 (1/1000, HPA023040, Atlas antibodies), S100A2 (1/200, HPA062451, Atlas antibodies), KRT7 (1/2000, ab181598, Abcam), DCLK1 (1/500, ab109029, Abcam), CD142 (1/100, AF2339, RandD), OLFM4 (1/5000, HPA077718, Atlas antibodies), MUC6 (1/4000, ab223846, Abcam), KI67 (1/1000, 14-5698-82, Ebioscience, Thermo Fisher Scientific), NANOG (1/200, 49035, Cell Signalling Technology, Danvers, Massachusetts, USA) and OCT3/4 (1/200, 561556, BD Biosciences, Franklin Lakes, New Jersey, USA). The next day, slides were incubated with a cocktail of secondary antibodies for 1 hour. Antibodies used were donkey anti-mouse Cy3 (1/500), donkey anti-mouse AF647 (1/500), donkey anti-rabbit AF647 (1/500), donkey anti-chicken Cy3 (1/100), donkey anti-rat AF647 (1/500), donkey anti-goat AF647 (1/500) and donkey anti-rabbit AF488 (1/500), all from Jackson ImmunoResearch (Ely, UK). After rinsing, slides were mounted with fluorescent mounting medium with DAPI added at 10 µg/ml. A section of human skin was included as positive control for ΔNp63.

RNA in situ hybridization (BaseScope)

For the BaseScope analysis, the standard protocol for BaseScope on FFPE tissue from ACDBio (Newark, California, USA) was used with the Basescope RED v2 kit. In short, 5µm slides were baked and deparaffinized, slides were incubated with hydrogen peroxide and next target retrieval was performed for 15 minutes. Protease III was applied for 15 minutes, and then the probe was incubated for 2 hours. A custom probe was designed to bind specifically to the promotor region of the delta isoform of P63, therefore not detecting the TA isoform. Standard hybridization followed, completed by signal detection and subsequent haematoxylin counterstaining. Slides were mounted with Pertex mounting medium.

FLIP-IT

FFPE processing

Samples were verified for P63 presence in 2D sections. 5mm punches (up to 37 mm^3 of tissue) were acquired with the Tissue-Tek Quick-Ray Tissue Microarray System (Sakura, Torrance, USA). The paraffin was visually eliminated from the punches using a heater at 65°C and then incubated in Hemo-De (Laborimpex 23412-01) overnight at room temperature. Afterwards samples were incubated in ethanol and rehydrated with 1xPBS-Triton 0,5%. Then washed for 3 incubations in 1xPBS-Triton 0,5%. All incubation steps were performed on an orbital shaker unless stated otherwise.

Delipidation

Samples were incubated with clearing solution consisting of 10% sodium dodecyl sulfate and 200mM boric acid pH7 at 45°C (human) or 54°C (mouse) for 3 days. The clearing solution was refreshed every day. Samples were washed 3x1h at room temperature (RT) with PBS-Triton 0,5% to rinse out remaining micelles.

Blocking and immunostaining

Samples were blocked overnight in blocking solution with 1x PBS-Triton 0,5% containing 25% casein block (Thermo Fisher Scientific, 37528) pH 7,5.

Immunostaining FLIP-IT

Samples were incubated with primary antibody solution containing 1xPBS-Triton 0,5%, 25% casein block for 3 days. Primary antibodies used: KRT5 (1/200, ab52635, Abcam), KRT7 (1/100, ab181598, Abcam), TROMAIII (1/50, DSHB), P63 (1/50, ab735, Abcam) and Laminin (1/25, L9393, Merck, Kenilworth, New Jersey, USA). After primary antibody incubation, samples were washed three times with wash buffer 1xPBS-Tween 0,2% containing 0,1% Heparin (LEO Pharma, Lier, Belgium) pH7,5 for 1 hour each and then incubated with 1/100 diluted Alexa Fluor donkey anti-mouse 647-, anti-rat Cy3-, and anti-rabbit 488-conjugated secondary antibody in wash buffer for 3 days. Next, samples were washed 3 times with washing buffer for 1 hour. All steps were performed at room temperature while samples were gently shaken in amber 5mL tubes (Eppendorf, Aarschot, Belgium) to protect the samples from light.

Refractive index matching and agarose gel embedding of the cleared tissue

FFPE samples were incubated in 50% and 100% CUBIC-R for at least 6h each2% CUBIC-R agarose was made by dissolving low melting point agarose powder (Sigma-Aldrich, A4018) in Fresh CUBIC-R in the microwave. To form the bottom gel layer (2mm height), 0.304mL of the solution was transferred with a P1000 pipette (Eppendorf) in a custom-made glass chamber, covered with a cover glass (Leica, Wetzlar, Germany) and incubated at 4°C for 15 minutes. To form the middle gel layer, 1.5mL of the mixture was poured into a 5mL tube to which the sample was added and carefully poured in the chamber and incubated at 4°C for 30 minutes. To form the top gel layer, the remaining mixture was poured in the chamber until the surface protruded slightly, covered with a cover glass, and incubated at 4°C for at least 30 minutes. The sample was then removed from the chamber and CR-ECi was started by immersion of the agarose block in 50% MilliQ-diluted CUBIC-R for at least 6h followed by 100% at least 12h. Next, the sample was dehydrated in ascending ethanol solutions (25,50,75,2x100%; each 30min with last incubation overnight) and subsequently incubated in ascending ECi solutions (25,50,75,2x100%; each 30min). The next day the sample was glued to the mount with superglue. All steps were performed while being protected from light as much as possible. The sample was immersed in fresh ECi for LSFM image acquisition.

LSFM Imaging

Images were acquired using a Zeiss Lighsheet Z.1 (Zeiss, Oberkochen, Germany) fitted with 405,488,561,638nm lasers. Samples were optically sectioned using a z-plane optimally adjusted. Overview images were acquired using 20x objective, NA=1 with zoom 0.36 – 8bit. High magnification

images were acquired using 20x objective with zoom between 1 and 2,5 (magnification 20x and 50x)-16bit.

Additional information FLIP-IT

Human samples

For FFPE samples, the complementary effect of CUBIC-R and FDA-approved optical clearing agent ECi allowed safe handling, versatile imaging, storage, transport and retention of fluorescence intensity over longer periods of time. Hong et al. were able to clear thick (0.5cm) fresh/FFPE human pancreatic samples using a modified iDISCO method. They used liquid dibenzyl ether (DBE) which we refrained from using since dipping high magnifying objectives in DBE could dissolve the glues within the objectives. Moreover, the iDISCO protocol induces severe sample shrinkage which to some extent would distort our assessments. Hence, we devised a novel methodology, FLIP-IT, that yielded consistently transparent pancreas samples ready for LSFM within two weeks, whether applied to fresh or FFPE stored specimens (some over 25 years old) and without sample shrinkage. The duration does not take into account required imaging time which is considerably longer for confocal microscopy.

Furthermore FLIP-IT allows the complete undisturbed imaging in agarose as it is compatible with CUBIC-agarose embedding. Regular water-agarose embedding results in opacity when using FFPE tissues. The opacity creates more refraction in the sample and subsequently imaging artefacts. This compatibility allows to image the complete sample without compromise (due to the use of glue directly on the sample).

We provide the adjacent figure showing FLIP-IT delipidation of fresh-fixed normal human pancreas. FLIP-IT is superior to FLASH (CLARITY-derived) and CUBIC-HL as the delipidation buffer retains sample integrity and size whereas FLASH and CUBIC HL induce shrinkage and take longer for homogenous delipidation.

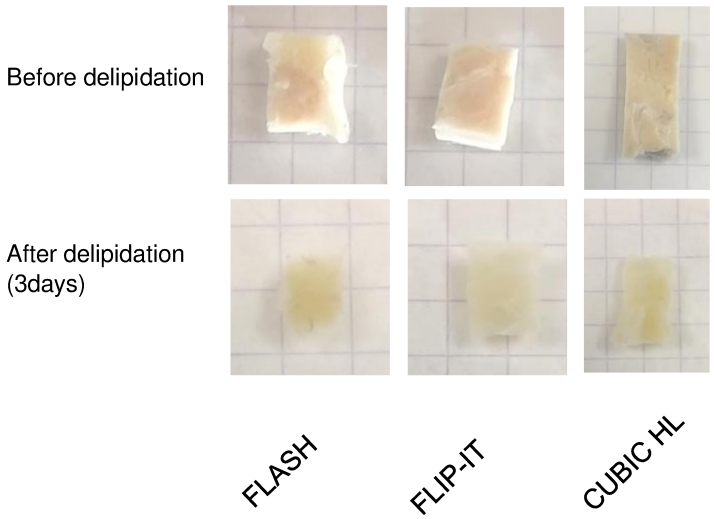

Mouse samples

Messal et al. used methyl salicylate for RI-matching again dissolving glues when using dipping objectives (1). Dipping objectives are required for high resolution light sheet fluorescence microscopy. The duration in S Fig 7 does not take into account required imaging time which is considerably longer for confocal microscopy. Additionally should the microscope be resistant to methyl salicylate the room would require additional hoods to eliminate the hazardous odor which is not require for ECi.

Within the FLASH protocol there is no indication whether it is suited for FFPE samples. The effect of methyl salicylate on FFPE processed tissue for LSFM has not yet been clarified.

For further in depth comparison as well as the comparison with other methods, we like to draw the attention to the publication of Messal et al. Nature protocols 2020 (1)-extended data figures 3,5-8 showing the comparison between the different protocols in fresh-fixed mouse pancreas, brain, mammary gland, lung and liver. The scope of our paper is centered around the use of formalin-fixed paraffin-embedded human pancreas hence we investigated the additional benefit of in particular FLASH (CLARITY), iDISCO, CUBIC clearing principles in this approach. Please note that FLASH and CLARITY are related in terms of clearing buffer (SDS-based) but due to the principle going back to CLARITY we tend to see FLASH as a major modification on the original CLARITY protocol. Where we place the FLIP-IT as a major enhancement of the FLASH (especially in regards to FFPE samples).

We provide the adjacent figure showing FLIP-IT delipidation of fresh-fixed mouse pancreas still attached to spleen and duodenum to maintain correct anatomical orientation. Although FLIP-IT and FLASH use the same delipidation buffer for mouse samples, the FLASH is not permissible for LSFM machines due to the manner of aggressive solvent for optical sample clearing.

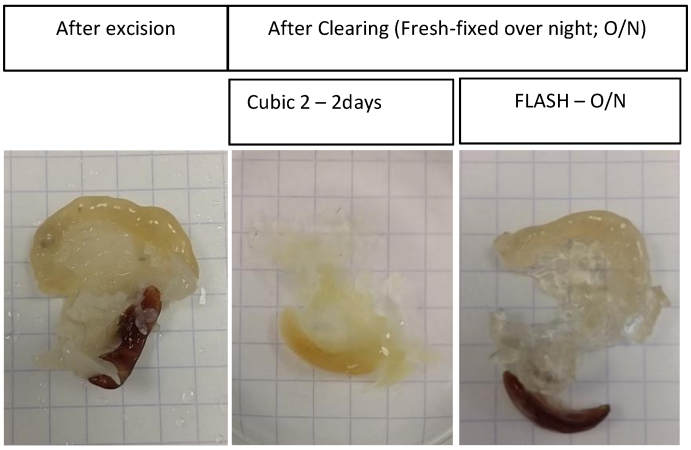

Dissociation and FACS analysis of pancreatic cells

Adult mouse pancreas from Sox9: eGFP transgenic mice (2) were harvested and digested in 1.4 mg/mL collagenase-P (Roche) at 37 °C for 20-30 min. Peripheral acinar-ductal units, depleted of endocrine islets, were prepared as described in (3). Following multiple washes with HBSS supplemented with 5% FBS, collagenase-digested pancreatic tissue was filtered through 600µm and 100µm poly-propylene mesh (BD). Peripheral acinar-ductal units containing intercalated ducts and centroacinar cells (hereinafter called small ducts of less than 100µm), intercalated (inter- and intra-lobular ducts, hereinafter called medium ducts of 100-µm) and main ducts and its ramifications (hereinafter called big ducts of more than 500µm) were further dissociated for FACS analysis in TrypLE (Invitrogen, Thermo Fisher Scientific) and incubated at 37 °C for 5 min. Dispersed cells were filtered through 40µm poly-propylene mesh (BD). Dissociated cells were then resuspended at 1:106 cells per ml in HBSS supplemented with 0.5% FBS. Cell sorting was performed using a FACS-Aria II (BD). The sorting gate for Sox9:eGFP positive ductal cells was established by using a WT mouse pancreas sample as negative control. Cells were directly sorted in RNeasy lysis buffer (Qiagen, Hilden, Germany) for RNA extraction or sorted in complete organoid media for culture.

Organoid culture

Entire ducts were embedded in GFR Matrigel, and cultured in organoid expansion medium (4) (AdDMEM/F12 medium supplemented with HEPES (1x, Invitrogen), Glutamax (1x, Invitrogen),

penicillin/streptomycin (1x, Invitrogen), B27 (1x, Invitrogen), N-acetyl-L-cysteine (1 mM, Sigma-Aldrich, RSPO1-conditioned medium (10% v/v), Noggin-conditioned medium (10% v/v), epidermal growth factor (EGF, 50 ng/ml, Peprotech, London, UK), Gastrin (10 nM, Sigma-Aldrich) and fibroblast growth factor 10 (FGF10, 100 ng/ml, Preprotech). After 3 passages we used the organoids for RNA or immunolocalization analysis. For genetic manipulation TP63 siRNA (NM_011641, Sigma-Aldrich) and the Thermo Fisher's Lipofectamine 3000 Transfection Kit (L3000-008) were used. In short, organoids were enzymatically disintegrated into single cells. Single cells were incubated with the lipofectamine 3000-siRNA mix for 4 hours at 37°C. After incubation, single cells were re-embedded in GFR Matrigel. Organoids were harvested 48 hours after genetic manipulation for RNA.

Cell lines and PDAC primary culture

HPDE cell line was purchased from Kerafast (Boston, USA). Cells were cultured in Keratinocyte Serum Free Medium, supplemented with Bovine Pituitary Extract and EGF (all from Thermo Fisher Scientific) in a humidified incubator at 37°C and 5% CO_2, according to previously published protocol (5). Cells were plated in a 6-well plate at a confluency of 70-80%, 24 hours prior to transfection. For the silencing of ΔNp63, a customized siRNA was designed at IDT (Iowa, USA) and three other validated siRNA's against full TP63 (TP63 TriFECTa DsiRNA kit, IDT) were tested. In short, 10nM of the siRNA diluted in opti-MEM was added to lipofectamine RNAiMAX(1:10 diluted in Opti-MEM). siRNA-lipofectamine RNAiMAX complexes were added to the well and incubated for a minimum of 4 hours. After 4 hours medium containing the complex was removed and replaced with complete medium. RNA and protein were collected 48 hours after transfection.

PDAC primary cell cultures were derived from 44 PDTX samples as described in (6). Briefly, PDX samples were split into several small pieces (1 mm^3) and processed in a biosafety chamber. After a fine mincing, they were treated with collagenase type V (C9263; Sigma-Aldrich) and trypsin/EDTA (25200-056; Gibco, Sigma-Aldrich) and suspended in DMEM supplemented with 1% w/w penicillin/streptomycin (Gibco, Life Technologies) and 10% of fetal bovine serum (Lonza, Bazel, Switzerland). After centrifugation, cells were re-suspended in Serum Free Ductal Media (SFDM) and conserved at 37°C in a 5% CO_2 incubator.

RNA analysis

Total RNA from organoids was isolated using the RNeasy Minikit (Qiagen) or TRizol followed by DNAse I treatment (Invitrogen) RNA was reverse transcribed with SuperScript III Reverse Transcriptase and random hexamers according to the manufacturer's instructions. qPCR of reverse-transcribed RNA samples was performed on a 7900 Real-Time PCR system (Applied Biosystems, Waltham, Massachusetts, Verenigde Staten) using the Power SYBR Green reagent (Applied Biosystems).

Total RNA from HPDE's was extracted with the NucleoSpin RNA isolation kit (Machery-Nagel, Düren, Germany), according to manufacturer's protocol. RNA concentration was measured using the NanoDrop 2000 (Thermofisher). Total RNA was reversed transcribed into cDNA using the GoScript Reverse Transcription System (Invitrogen). qPCR was performed using FastSYBRGreen 5× MasterMix on a QuantStudio 6 (Invitrogen). Primers were obtained from IDT. Analysis was done by determination of the comparative threshold cycle. For normalization GAPDH and HPRT were used.

PDAC Primary cultures total RNA was extracted using RNeasy mini kit (Qiagen). mRNA profiles were obtained using Illumina's TrueSeq Stranded mRNA LT protocol. Sequencing followed oligo-dT capture and was done on a paired-end 100 pair flow cell. mRNA libraries were prepared and sequenced by AROS Applied Biotechnology A/S (Aarhus, Denmark). RNAseq reads were mapped using STAR 18 with the proposed ENCODE parameters) and SMAP on the human hg19 and mouse mmu38 genomes and

transcript annotation (Ensembl 75). Gene expression profiles were obtained using FeatureCount. Only genes with at least three read counts in at least 3 samples were kept for further analysis. Gene counts were normalized using the upper-quartile approach.

RNA sequencing and data analysis

Differential gene expression between HPDE knockdown and control was performed on the Illumnia NovaSeq 6000 instrument at the VIB, Nucleomics Core, Leuven, Belgium. Library prep was performed with the Truseq. Low quality ends (<Q20) were trimmed using FastX 0.0.14. Reads shorter than 35bp after trimming were removed. FastX 0.0.14 and ShortRead 1.40.0 were used to remove polyA-reads (more than 90% of the bases equal A), ambiguous reads (containing N), low quality reads (more than 50% of the bases < Q25) and artifact reads (all but 3 bases in the read equal one base type). Pre-processed reads were aligned to the reference genome of Homo sapiens (GRCh38). Expression levels were computed by counting the number of reads in the alignment that overlapped with gene features using featureCounts 1.5.3. Within and between sample normalization was conducted with the EDASeq package from Bioconductor. FMPK values were determined by dividing normalized counts by the total number of counts (in millions) for each sample. For each gene, the scaled counts were divided by the gene length (in kbp), resulting in the number of Fragments Per Kilobase of gene sequence and per Million fragments of library size. Differential gene expression between ΔNp63 KD and control was determined with the edgeR 3.24.3 package of Bioconductor.

Analysis of ΔNp63 isoform and correlation with molecular subtypes

To establish the link between Δnp63 specific isoform and the PDAC subtypes, transcriptome data from 44 primary cell cultures and 6 HPDE cells were used to determine their PAMG (7). Raw count quantification was performed using Kallisto quant tool (8) and Homo sapiens genome (GRCh38) from ENSEMBL database. Raw counts were normalized using the upper-quartile approach (9) and log2 transformed. The PAMG scores were obtained from transcriptomes by projection on the previously published molecular signature (7). Pearson's correlation test was used to evaluate the relationship between the expression level of Δnp63 isoform and PAMG. The classification into basal-like and classical subtypes was performed using the PurIST classifier (10).

Whole mount organoid staining

For whole mount organoid staining the protocol described in Dekkers et al. (11) was followed with minor modifications. Antibodies used were anti-SOX9 (Sigma-Aldrich AB5535) and anti-P63 (ab735, Abcam).

Immunostainings on HPDE cell pellet

KD and control samples were shortly centrifuged and fixed for 24 hours at room temperature in 4% paraformaldehyde. Cells were resuspended in pre-warmed agarose, centrifuged and embedded into paraffin. 4µm tissue sections were cut. For staining the abovementioned protocol for immunofluorescence was followed. Primary antibodies used were: anti-KRT5 (1/100, ab52635, Abcam), anti-P63 (1/50, ab735, Abcam) and anti-KRT19 (1/100, GA61561-2, Dako). Secondary antibodies used were: anti-rabbit AF647 (1/500) and anti-mouse Cy3 (1/500), both from Jackson.

Immunoblotting

Total protein samples were extracted using the RIPA buffer (150 mM NaCl, 1.0% Triton X-100, 0.5% sodium deoxycholate, 0.1% SDS and 50mM Tris pH 8.0), supplemented with Protease and phosphatase inhibitors (both from Sigma-Aldrich). Protein concentration was determined using the Bradford Assay

(Bio-Rad, Hercules, CA, USA). Samples were mixed with loading buffer (4% SDS, 20% glycerol, 10% ß-mercaptoethanol, 0.004% bromophenol blue, and 0.125M Tris-HCl pH 6.8), boiled for 5 minutes at 95°C, followed by short centrifugation at maximum speed for 1 minute at 4°C. Equal amounts of proteins were loaded on a 10% polyacrylamide gel and transferred overnight on a Nitrocellulose membrane. Membranes were blocked with Tris-Buffered Saline and Tween 20 (TBST) with 5% non-fat milk. After 1 hour of blocking, membranes were incubated overnight at 4°C with the primary antibodies in 3%BSA in TBS-T. Primary antibodies used were: anti-P40 (ABS552, Sigma-Aldrich, 1/500) and anti-β-actin (A1978, Sigma-Aldrich, 1/100). After washing, membranes were incubated with the secondary antibodies for 1 hour at room temperature. Secondary antibodies used were: anti-rabbit 800CW or anti-mouse 680RD (Li-Cor Biosciences, Lincoln, Nebraska, USA). Protein signal was visualized with the Li-Cor Odyssey Fc Imaging System.

Image acquisition and processing

DAB slides were visualized and scanned with the Aperio CS2, the 3DHistech Pannoramic SCAN slide scanner and Zeiss AXIOSCAN Z.1. Slides were viewed with the Pathomation PMA.view software.

Fluorescent multiplex stainings were visualized with EVOS FL Auto Cell Imaging System or Zeiss AXIOSCAN Z.1. Confocal imaging was done using the ZEISS LSM 800 system. A merged Z-stack was created and saved as a PNG using the ZEISS Zen Lite program. BaseScope slides were also imaged with the ZEISS LSM 800 system, using the Cy3 channel to detect the BaseScope signal, and the brightfield channel to detect the haematoxylin staining.

Acquisitioned 3D data was processed using Zen black software using online dualside fusion algorithm. If necessary DualsideFusion files underwent background subtraction or were deconvolved using deconvolution module set to medium strength constrained iterative deconvolution. Afterwards tiled images were imported in Arivis 3.0 for stitching. 3D renderings, movies and images were acquired using Arivis software.

Data analysis

The HALO image analysis platform was used for all quantifications of 2D slides. Prior to analysis, scans were cleaned for possible processing artifacts. To quantify the total ΔNp63$^+$ cells over all cells located in ducts, ducts were first annotated on one annotation layer and were then calculated using the multiplex IHC v3.0 quantification algorithm. To calculate the optical density of haematoxylin and eosin in ΔNp63$^+$ cells and duct cells, two annotation layers were created, and a selection of ΔNp63$^+$ cells and duct cells were annotated in a separate layer each. The optical density was quantified using the Area Quantification v2.1.3 algorithm. Finally, ΔNp63 expression in tumours was analysed on tissue microarrays (TMAs), which were first segmented using the TMA module and whole slides. ΔNp63 signal was quantified using the multiplex IHC v3.0. For the ΔNp63 quantification in murine samples, HALO AI was trained for nuclei and ductal morphology segmentation on 25% of used sections. HALO AI – nuclei phenotyper plugin was specifically applied on nuclei and ductal phenotype segmentation. Mouse skin tissue served as a positive training control. ΔNp63-KI67 co-expression was quantified using HALO AI - nuclei phenotyper plugin. All returned data underwent visual quality control.

Arivis v3.2 was used to analyze 3D high resolution images. Voxel operations, membrane segmentation and 3D object building pipelines were created in Arivis for identification of KRT7$^+$ and KRT5$^+$ cells while excluding cells touching the edges. Membrane segmenter was set to plane-wise segmentation allowing holes and full connectivity in X/Y/Z. The segments were interrogated for Sphericity (3D roundness/shape) and volume. Manual quality control was performed for omittance of false-positive and -negative results.

H-scoring

125 cases of PDAC were analyzed using the ΔNp63 immunostaining to assess the extent of nuclear immunoreactivity of ΔNp63 in the cancer cells, the H-score was applied. Only cancer cells with a clear invasive growth were analyzed (N=122). All non-cancerous areas and areas with carcinoma in situ were excluded from analysis. All images were scanned and digitally reviewed by a trained pathologist using the HALO 3.2 software.

Intensity of positive nuclear staining of the cancer cells was determined according the following scheme: 0, no nuclear staining of cancers cells; 1+, weak nuclear staining; 2+, moderate nuclear staining; 3+, strong nuclear staining The H-score was obtained by the formula: 3 x percentage of strongly staining nuclei + 2 x percentage of weak/moderately staining nuclei + percentage of faint staining nuclei, giving a range of 0 to 300.

Statistical analysis

Experimental data were analysed by two-tailed unpaired Student t test, unpaired t test with Welch's correction, paired t-test, Mann–Whitney or one-way Anova with Turkey's multiple comparisons test using GraphPad Prism8.0 and statistical significance was accepted at $P < 0.05$. The results are shown as mean ± standard error of mean (SEM). The number of independent experiments (n) is indicated in the figure legends. We tested positive rate and prevalence using meta-analysis and Clopper-Pearson.

List of primers

Primer	Species	Sequences
GAPDH	Human	Forward: TGC ACC ACC AAC TGC TTA GC
		Reverse: GGC ATG GAC TGT GGT CAT GAG
HPRT	Human	Forward: GGC TCC GTT ATG GCG ACC C
		Reverse: TGT GAT GGC CTC CCA TCT CCT T
DeltaNP63	Human	Forward: AGC CAG AAG AAA GGA CAG CA
		Reverse: CAG GTT CGT GTA CTG TGG CT
KRT5	Human	Forward: CGT GCC GCA GTT CTA TAT TCT
		Reverse: ACT TTG GGT TCT CGT GTC AG
KRT19	Human	Forward: CCTCCCGCGATTACAACCACT
		Reverse: GGCGAGCATTGTCAATCTGT
SOX9	Human	Forward: AGA TGT GCG TCT GCT C
		Reverse: CTC TGG AGA CTT CTG AAC G
HNF1β	Human	Forward: TACGACCGGCAAAAGAATCC
		Reverse: TGCGAACCAGTTGTAGACACG

References

1. Messal HA, Alt S, M Ferreira rute M, Gribben C, Min-Yi Wang V, Cotoi CG, et al. Tissue curvature and apicobasal mechanical tension imbalance instruct cancer morphogenesis. Nature.

2. Gong S, Zheng C, Doughty ML, Losos K, Didkovsky N, Schambra UB, et al. A gene expression atlas of the central nervous system based on bacterial artificial chromosomes. Nature. 2003;425(6961):917–25.

3. Wang YJ, Bailey JM, Rovira M, Leach SD. Sphere-Forming Assays for Assessment of Benign and Malignant Pancreatic Stem Cells. In: Methods in Molecular Biology. 2013. p. 281–90.

4. Boj SF, Hwang C-I, Baker LA, Chio IIC, Engle DD, Corbo V, et al. Organoid Models of Human and Mouse Ductal Pancreatic Cancer. Cell. 2015;160(1–2):324–38.

5. Furukawa T, Duguid WP, Rosenberg L, Viallet J, Galloway DA, Tsao MS. Long-term culture and immortalization of epithelial cells from normal adult human pancreatic ducts transfected by the E6E7 gene of human papilloma virus 16. Am J Pathol. 1996 Jun;148(6):1763–70.

6. Kaoutari A El, Fraunhoffer NA, Hoare O, Teyssedou C, Soubeyran P, Gayet O, et al. Metabolomic profiling of pancreatic adenocarcinoma reveals key features driving clinical outcome and drug resistance. EBioMedicine. 2021 Apr;66:103332.

7. Nicolle R, Blum Y, Duconseil P, Vanbrugghe C, Brandone N, Poizat F, et al. Establishment of a pancreatic adenocarcinoma molecular gradient (PAMG) that predicts the clinical outcome of pancreatic cancer. EBioMedicine. 2020 Jul;57:102858.

8. Bray NL, Pimentel H, Melsted P, Pachter L. Near-optimal probabilistic RNA-seq quantification. Nat Biotechnol. 2016 May;34(5):525–7.

9. Bullard JH, Purdom E, Hansen KD, Dudoit S. Evaluation of statistical methods for normalization and differential expression in mRNA-Seq experiments. BMC Bioinformatics. 2010 Feb;11:94.

10. Rashid NU, Peng XL, Jin C, Moffitt RA, Volmar KE, Belt BA, et al. Purity Independent Subtyping of Tumors (PurIST), A Clinically Robust, Single-sample Classifier for Tumor Subtyping in Pancreatic Cancer. Clin cancer Res an Off J Am Assoc Cancer Res. 2020 Jan;26(1):82–92.

11. Dekkers JF, Alieva M, Wellens LM, Ariese HCR, Jamieson PR, Vonk AM, et al. High-resolution 3D imaging of fixed and cleared organoids. Nat Protoc. 2019;14(6):1756–71.